Multiple Landmark Acquisition and Tracking Using Variable Speed and Classical CMGs On-board Spacecraft

Abhilash Mony *
Indian Space Research Organisation, Trivandrum, Kerala 695013, India

Hari Hablani †
Indian Institute of Technology Indore, Madhya Pradesh 453552, India

Aditya Paranjape.‡
Imperial College London,South Kensington Campus, London SW7 2AZ, UK

It is well known that the high torque output of CMGs is affected by its geometric singularities. In Variable Speed Control Moment Gyros (VSCMGs), the changing wheel speed gives an extra degree of freedom per CMG to avoid or escape singular conditions. The effectiveness of utilizing a cluster of VSCMGs for multiple landmark acquisition and tracking has not been covered in literature. This is investigated in this paper and compared with the performance of a constant speed CMG cluster. For the same target sequence and a time optimal outer-loop attitude controller, roof-type 4-CMG clusters with constant or variable wheel speed are used to acquire and track multiple targets. The efficacy of the actuators under various steering laws is compared based on the metrics- normalized torque and momentum errors, singularity index, residual attitude errors, feasibility of realizing the computed gimbal rates and total energy consumed. The performance CMG and VSCMG steering laws with and without null motion are investigated. The CMG singular direction avoidance steering law with null motion gives enhanced time of payload operation (by 2 seconds), gives smoother gimbal rates, produces 62.5% **less momentum error and consumes** 13% **less energy relative to the VSCMG steering with null motion.**

*Section Head, Advanced Actuators and Mechanisms Section, ISRO Inertial Systems Unit, Email: abhilash.mony@gmail.com
†Professor, Astronomy, Astrophysics and Space Engineering, IIT-Indore, Email: hbhablani@iiti.ac.in. Associate Fellow, AIAA.
‡Lecturer,Department of Aeronautics, Imperial College; Email: a.paranjape@imperial.ac.uk. Senior Member, AIAA.

Nomenclature

a_i	=	maximum acceleration about the i^{th} axis, $i = x, y, z$
$\boldsymbol{b}$	=	payload bore-sight unit vector in body frame
d	=	scalar scaling term for assigning weight to the null gimbal rates
$\boldsymbol{D} \in \mathbb{R}^{3\times N}$	=	Jacobian matrix of the N-CMG cluster
$\boldsymbol{Q} \in \mathbb{R}^{3\times 2N}$	=	Jacobian matrix of the N-VSCMG cluster
$\hat{\boldsymbol{e}}$	=	Euler axis
$\mathbf{F}$	=	Frames of reference - Inertial, Local-Vertical-Local-Horizontal, Body etc.
$\hat{\boldsymbol{g}}, \hat{\boldsymbol{g}}_t, \hat{\boldsymbol{g}}_g$	=	unit vectors on the gimbal frame F^G along the spin, torque and gimbal axes, respectively
h	=	magnitude of the individual CMG angular momentum
$\boldsymbol{H}$	=	angular momentum vector
$\boldsymbol{J}, J$	=	Inertia matrix and (scalar) moment of inertia along a particular axis
$\boldsymbol{L}$	=	torque-control,disturbance,gyric
m	=	singularity index
T_{max}	=	maximum achievable output torque
$\boldsymbol{u}_l$	=	line-of-sight unit vector in the LVLH frame
$[\boldsymbol{\omega}\times]$	=	skew symmetric cross product matrix consisting of elements of $\boldsymbol{\omega}$, in rad/s
α	=	scalar term which depends on the singularity index
γ,$\boldsymbol{\gamma}$	=	gimbal angle and vector of gimbal angles
ϕ_q	=	angle of rotation about the Eigen axis in radians
$\boldsymbol{\tau}$	=	torque demand from the controller
$\boldsymbol{\omega}$	=	inertial body rates of the spacecraft
Ω	=	CMG wheel rotation speed in radians per second
W_{s_i},W_{g_i}	=	weights assigned for wheel acceleration and gimbal rate resp.
κ	=	Condition number of the Jacobian matrix, $\mathbf{D}$

I. Introduction

The high torque capability of single-gimbal Control Moment Gyros (CMGs) makes them an attractive choice for spacecraft which demand rapid manoeuvres from one attitude to another. Such low-earth remote sensing spacecraft will have body mounted payloads. Realization of large actuator torques helps in large off-nadir pointing quickly and provides spot-to-spot acquisition capabilities. Such capabilities help in collecting more data per orbit, reduce the revisit time, and enable rapid multi-target acquisition and tracking. Typical Reaction Wheels(RWs) have output torque in

the range of 0.03 N.m-0.4 N.m [1, 2]. On the other hand, CMGs can easily generate torque output of the order of 15 N.m-75 N.m. The commercially available CMGs developed by Honeywell and Airbus have maximum torque output capability of 75 N.m and 45 N.m respectively [3, 4]. The high torque capability of CMG is impaired by occasional geometric singularities. This makes its steering law complicated. RWs have a non-gimballed torque output about the spin axis and can thus be used with simpler algorithms.

A. Overview of the literature

The geometric singularity problem of CMG has been thoroughly investigated in the literature [5–10]. The geometric theory of CMG singularities based on differential geometry was first studied in [8]. In these studies, the CMG singularities were classified as elliptic and hyperbolic. The mechanical simplicity and torque amplification effect of single-gimbal CMGs motivated the development of steering laws for it.

There are singularity escape and avoidance laws. The singularity-escape algorithms are designed to pass through, if inevitable, and hence escape from, the singularities with nonzero torque error while the singularity avoidance algorithms induct null motion which, by definition, do not cause a torque error. A null motion introduces gimbal rates, without generating a torque, proportional to the gradient of the singularity index relative to the gimbal angles or even use the gimbal angles directly. While this technique avoids non-degenerate hyperbolic singularities, it is ineffective in avoiding internal elliptic singularities [7].

The singularity escape laws are all modifications of the classical Moore-Penrose pseudoinverse solution of the CMG angular momentum Jacobian like Singularity Robust Inverse (SRI) [5, 11], Generalized Singularity Robust Inverse (GSR) [9], Universal Steering law (USL) [10], Singular Direction Avoidance Law (SDA) [12]. The avoidance of singularity using null motion has also been explored in [5, 7].

A combination of singularity avoidance and escape steering law was put forward as a Hybrid Steering Law by Leve et al. [13]. This avoided hyperbolic singularities with null motion and elliptic singularities with some minimal, acceptable torque error by assigning appropriate weightage to the singularity escape and null motion steering laws depending on the type of singularity. A set of initial gimbal angles (termed as Preferred Gimbal Angles) to avoid CMG singularity was introduced by Vadali et al in [14]. It was then demonstrated through simulations that CMG cluster when started from these set of preferred gimbal angles tends to avoid the internal singularities and takes the cluster towards its saturation limit (saturation singularity). A form of null motion using a set of desired gimbal angles was introduced by Lappas et al. in [15]. By treating singularity as an obstacle, a motion planning based singularity avoidance of a 4-CMG cluster in the attitude space of the satellite was demonstrated in [16].

The VSCMG with spacecraft dynamics is well explained in [17] which described the acceleration and velocity based steering laws. The VSCMG null motion steering laws are given in [18]. Here unlike constant speed CMGs, the wheel speeds are also changed along with the gimbal angles. In theory, VSCMGs with the extra degree of freedom

provided by the wheels are better equipped to avoid singular configurations. The classification of singularity as in constant speed CMGs are not defined rigorously in case of VSCMGs.

Two types of VSCMG null motion based on preferred gimbal angles and gradient of the condition number are explained in [18]. Using a weighted pseudo-inverse steering law, the wheel torques are produced only when the CMG cluster operates close to a singular configuration. Hence, ideally, by varying their wheel spin speeds, the VSCMGs should be able to generate the torque and pass through the singular conditions. Hence VSCMG steering algorithm can be classified under singularity escape steering laws.

B. Contributions

The full capability of the CMGs can be utilized on satellites which demand a fast manoeuvre from one attitude to another. Many steering laws exists for CMGs. In addition VSCMG control laws have been introduced and shown to be superior due to the extra degrees of freedom available from the wheel [18]. Except for the examples shown in [9, 19] for multiple rest-to-rest manoeuvres, all steering laws have been demonstrated for simple one step rest-to-rest manoeuvre. This condition can not reveal the advantages or disadvantages of the steering laws. Hence it was felt that for evaluating the performance of a CMG/VSCMG cluster, and to find the effectiveness of their corresponding steering laws, the ability to execute a series of time-optimal track-to-track manoeuvre will be highly insightful. These results will be extremely useful, especially for practicing attitude control engineers.

In this paper, the effectiveness of a cluster of CMGs to complete this manoeuvre is demonstrated by using a combination of singularity avoidance and escape steering laws from the ones mentioned earlier. The performance of three VSCMG steering laws-classical VSCMG steering law and its combination with two different type of null motion is studied to evaluate their effectiveness in executing a multiple landmark acquisition and tracking manoeuvre.

The primary contribution of this work is to apply and compare these steering laws in the context of a realistic spacecraft manoeuvre. The performance across constant and variable speed CMGs and their steering logics are compared for their ability to track the commanded torque in terms of normalized torque and momentum errors, their singularity index and residual attitude errors. The ability to realize the computed gimbal rate and the total energy consumed are also compared. The VSCMG laws are implemented such that the demanded wheel torques are realizable. This is pertinent because the VSCMG steering laws can not be practically used if large torques are demanded from VSCMG wheels about the spin axes while performing the manoeuvre. The study determines whether the VSCMGs, with their extra degrees of freedom truly improve the tracking performance compared to the constant speed CMGs while executing multiple landmark acquisition and tracking manoeuvre. It also compares their effectiveness holistically, by comparing multiple performance parameters

C. Organization

The paper is organized as follows. The kinematics of landmark acquisition and tracking problem is introduced in Sec. II. The commanded quaternions and rate commands are derived here based on the spacecraft-target geometry. The attitude dynamics and control of a spacecraft equipped with VSCMGs is summarized in Sec. III.The particulars of the time-optimal attitude controller used are also explained in Sec. III. This is followed by the details regarding the VSCMG and CMG steering laws and their null motion combinations in Sec. IV. Numerical simulation results of multiple landmark acquisition and tracking using various CMG and VSCMG steering laws with and without null motion are presented in Sec. V. The observations and inferences for each steering law is also explained here. In Sec. VI, a comparison across all the steering laws studied is illustrated. The discussion in Sec. VII concludes the paper.

II. Kinematics for Landmark Acquisition and Tracking

A. Introduction

Landmark acquisition involves pointing of spacecraft payload to a particular location of interest. Mathematically, the payload bore-sight unit vector $\boldsymbol{b}$, fixed in the spacecraft body frame $\mathbf{F^b}$ in the present application, has to be pointed in the direction of a desired line-of-sight unit (LoS) vector $\boldsymbol{u}_l$. First, the target LoS vector has to be calculated from the spacecraft-target geometry followed by the computation of the commanded quaternions. Once the target is acquired, it has to be tracked based on the relative motion between the spacecraft and the earth. This is derived based on the rate of change of the LoS vector. The calculation of the target LoS unit vector, commanded quaternion and commanded tracking rates are well explained in [20]. The standard attitude kinematic equations for quaternion propagation are used. The error quaternion, which represents the error from the current to the commanded quaternion is taken from [21].

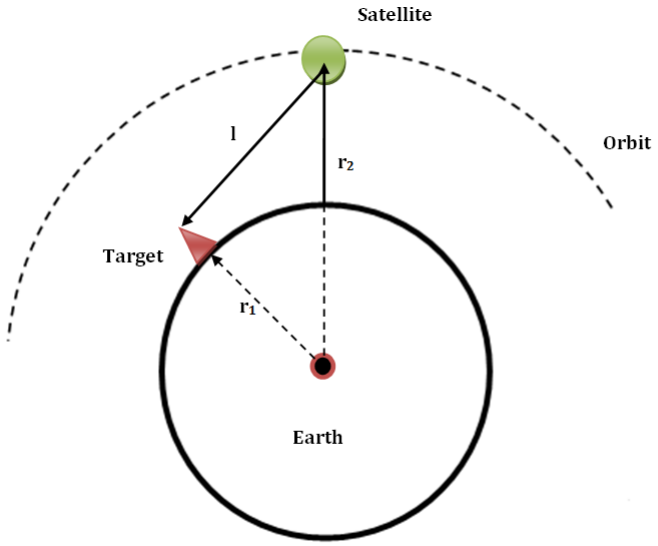

Fig. 1 Line-of-sight vector of the target from spacecraft based on geometry

B. Target LoS Vector

Consider a spacecraft in low-earth orbit as shown in Fig. 1. The target position vector $\mathbf{r_1}^{\mathbf{F}^I}$ and position vector of the spacecraft $\mathbf{r_2}^{\mathbf{F}^I}$ with respect to the earth-centered inertial (ECI) frame $\mathbf{F^I}$ are shown. From the geometry, the line-of-sight vector from the spacecraft to the target can be written as stated in (1).

$$\mathbf{l}^{\mathbf{F}^I} = -\mathbf{r_2}^{\mathbf{F}^I} + \mathbf{r_1}^{\mathbf{F}^I} \tag{1}$$

Position vector of $\mathbf{r_2}^{\mathbf{F}^I}$ can be expressed in terms of the orbital parameters as given in [22] and $\mathbf{r_1}^{\mathbf{F}^I}$ in terms of latitude and inertial longitude as given in [20]. The line-of-sight unit vector in the inertial frame, $\hat{\mathbf{u}}^{\mathbf{F^I}}$, is given in (2).

$$\hat{\mathbf{u}}^{\mathbf{F^I}} = \frac{\mathbf{l}^{\mathbf{F}^I}}{\|\mathbf{l}^{\mathbf{F}^I}\|} \tag{2}$$

$$\mathbf{r_2}^{\mathbf{F}^I} = r_{sat} \begin{pmatrix} cos(\omega_{ar}+\nu)cos(\Omega_R) - sin(\omega_{ar}+\nu)cos(i)sin(\Omega_R) \\ cos(\omega_{ar}+\nu)sin(\Omega_R) + sin(\omega_{ar}+\nu)cos(i)cos(\Omega_R) \\ sin(\omega_{ar}+\nu)sin(i) \end{pmatrix} \tag{3}$$

$$\mathbf{r_1}^{\mathbf{F}^I} = r_{earth} \begin{pmatrix} cos(\lambda_{Lat})cos(\alpha_{Lon}) \\ cos(\lambda_{Lat})sin(\alpha_{Lon}) \\ sin(\lambda_{Lat}) \end{pmatrix} \tag{4}$$

where ω_{ar}= argument of perigee, ν = true Anomaly, Ω_R=right ascension of ascending node, i = inclination angle, α_{Lon}=inertial longitude of the target (geographic longitude+ Greenwich hour angle), λ_{Lat} = latitude of the target, r_{earth} = radius of the earth and r_{sat} = radius of the spacecraft orbit.

The line-of-sight(LoS) vector thus obtained is transformed to the local-vertical-local-horizontal frame (LVLH frame or $\mathbf{F^{lvlh}}$) by a series of transformation as given in [20]. Let this be represented by the 3×3 transformation matrix $\mathbf{C}_{lvlh-ECI}$. The LoS unit vector in $\mathbf{F^{lvlh}}$ frame is defined as $\boldsymbol{u}_l$ and is computed as in (5).

$$\mathbf{u}_l = \mathbf{C}_{lvlh-ECI}\ \ \hat{\mathbf{u}}^{\mathbf{F^I}} \tag{5}$$

C. Quaternion Pointing Commands from LoS

Let the quaternion command to point the spacecraft payload bore-sight unit vector $\boldsymbol{b}$ to the target be denoted as $\boldsymbol{q}_c$. To align $\boldsymbol{b}$, defined in the $\mathbf{F^{lvlh}}$ frame with the unit vector $\mathbf{u}_l$, $\boldsymbol{q}_c$ is given as [23]

$$\boldsymbol{q}_c = \frac{1}{\sqrt{2\,(1+\boldsymbol{b}^\top \boldsymbol{u}_l)}} \begin{bmatrix} \boldsymbol{b} \times \boldsymbol{u}_l \\ 1 + \boldsymbol{b}^\top \boldsymbol{u}_l \end{bmatrix} \tag{6}$$

D. Tracking Rate Commands

After the target is acquired, the spacecraft is commanded to track the target. The inertial tracking rate is calculated in the body frame $\mathbf{F^b}$ using the line-of-sight vector $\mathbf{l}$ and its inertial rate thus [20]:

$$\boldsymbol{\omega_{cI}} = \frac{\mathbf{l} \times \dot{\mathbf{l}}}{l^2} \tag{7}$$

All the vectors in 7 are expressed in the body frame $\mathbf{F^b}$ and the superscript showing the same is dropped for brevity.

E. Attitude Kinematics

We use quaternions to represent the spacecraft attitude. Recall that the quaternion is written in terms of the direction of the Euler axis of rotation, $\hat{\boldsymbol{e}} = [e_1 \;\; e_2 \;\; e_3]^\top$ and the angle ϕ_q about the Euler axis. The four elements of a quaternion $\boldsymbol{q} = [q_1 \;\; q_2 \;\; q_3 \;\; q_4]^\top$ are given by:

$$q_4 = \cos(\phi_q/2),\; q_i = e_i \sin(\phi_q/2) \quad i = 1,2,3 \tag{8}$$

The quaternion kinematics is given by:

$$\dot{\boldsymbol{q}}_{1:3} = -\frac{1}{2}[\boldsymbol{\omega}\times]\boldsymbol{q}_{1:3} + \frac{1}{2}q_4\boldsymbol{\omega},\;\; \boldsymbol{q}_{1:3} = [q_1\, q_2\, q_3]^\top \tag{9a}$$

$$\dot{q}_4 = -\frac{1}{2}\,\boldsymbol{\omega}^\top \boldsymbol{q} \tag{9b}$$

where the matrix $[\boldsymbol{\omega}^\times]$ is the skew-symmetric cross product matrix defined as in [24].

Let the quaternion command be $\boldsymbol{q}_c = [q_{1c} \;\; q_{2c} \;\; q_{3c} \;\; q_{4c}]^\top$. The error quaternion, which represents the error from the current orientation to the commanded orientation is given as [19, 21, 25]:

$$\begin{bmatrix} q_{1e} \\ q_{2e} \\ q_{3e} \\ q_{4e} \end{bmatrix} = \begin{bmatrix} q_{4c} & q_{3c} & -q_{2c} & -q_{1c} \\ -q_{3c} & q_{4c} & q_{1c} & -q_{2c} \\ q_{2c} & -q_{1c} & q_{4c} & -q_{3c} \\ q_{1c} & q_{2c} & q_{3c} & q_{4c} \end{bmatrix} \begin{bmatrix} q_1 \\ q_2 \\ q_3 \\ q_4 \end{bmatrix} \tag{10}$$

F. Payload Bore-Sight Ground Trace

The payload bore-sight ground trace shows the mission performance of the satellite. It shows the payload bore-sight motion on the ground as it is maneuvered from one target to another and then dwells on the target during the payload operation phase. The sub-satellite ground trace analysis is covered in [22, 26]. Payload bore-sight intercept analysis is given in [27]. A comprehensive and systematic analysis of the same along with the results given in [28] are explained in [29, 30]. The final expressions are obtained after considerable algebra and hence are omitted here for brevity. The readers are encouraged to study the mentioned references for the details.

III. Spacecraft Attitude Dynamics and Control

A. Spacecraft Dynamics with Single-Gimbal VSCMGs

Following [18], Secs. 4.5 and 8.8, consider a rigid spacecraft with a cluster of $N > 1$ single gimbal VSCMGs. Let $\boldsymbol{J}_{sat}$ be the inertia tensor of the spacecraft and $\boldsymbol{\omega}$ its inertial body rate expressed in the body frame $\mathbf{F^b}$. Consider $\hat{\boldsymbol{g}}_s$, $\hat{\boldsymbol{g}}_t, \hat{\boldsymbol{g}}_g$ as orthogonal triad of unit vectors fixed in the gimbal frame $\mathbf{F^G}$ for the single VSCMG. The unit vectors are along the wheel spin axis, torque axis and gimbal axis, respectively, and are expressed in the spacecraft frame $\mathbf{F^b}$. By considering the combined angular momentum of the wheel, gimbal and spacecraft the attitude dynamic equations of a rigid spacecraft with N VSCMGs is given by [17, 18].

$$
\begin{aligned}
&\boldsymbol{J}_{sat}\dot{\boldsymbol{\omega}} = -[\boldsymbol{\omega}^{\times}]\, \boldsymbol{J}_{sat}\, \boldsymbol{\omega} + \boldsymbol{L}_{ext} \\
&- \sum_{i=1}^{N} (\{J_{s_i}\dot{\gamma}_i\omega_{t_i} + (J_{g_i} - J_{t_i})\dot{\gamma}_i\omega_{t_i} + J_{W_{si}}\dot{\Omega}_i\}\hat{\boldsymbol{g}}_{s_i}) \\
&- \sum_{i=1}^{N} (\{J_{s_i}\dot{\gamma}_i\omega_{s_i} - (J_{t_i} + J_{g_i})\dot{\gamma}_i\omega_{s_i} + J_{W_{si}}\Omega_i(\dot{\gamma}_i + \omega_{g_i})\}\hat{\boldsymbol{g}}_{t_i}) \\
&- \sum_{i=1}^{N} (\{J_{g_i}\ddot{\gamma}_i - J_{W_{si}}\Omega_i\omega_{t_i}\}\hat{\boldsymbol{g}}_{g_i})
\end{aligned}
\tag{11}
$$

J_{s_i}, J_{t_i} and J_{g_i} are the total inertia of the rotating elements of the i^{th} VSCMG along the spin axis, torque axis and the gimbal axis, respectively, in $\mathbf{F^G}$. Gimbal angle is denoted by γ_i and its derivatives denote the gimbal rate and acceleration. $J_{W_{si}}$ is the wheel spin axis inertia, Ω_i is the wheel rotation speed. The terms ω_{s_i}, ω_{t_i} and ω_{g_i} are the projections of the spacecraft body rate $\boldsymbol{\omega}$ onto the gimbal frame $\mathbf{F^G}$ for the i^{th} VSCMG. The term $\boldsymbol{L}_{ext}$ represents the external disturbance torque acting on the spacecraft. The terms $\dot{\Omega}_i$ and $\ddot{\gamma}_i$ represents the wheel and gimbal accelerations respectively. The former becomes significant for VSCMGs. By making this zero, we get dynamic equations of constant speed CMGs. Since the CMGs are controlled using gimbal rates, the terms related to the gimbal acceleration ($\ddot{\gamma}_i$) can be ignored. So to simplify 11, we ignore the terms related to $\ddot{\gamma}_i$ and group the terms with $\dot{\gamma}_i$ and $\dot{\Omega}_i$ [17, 18].

Let us define $\mathbf{D}_0$ containing the wheels moments of inertia about the spin axes and $\mathbf{D}$ representing the terms in

connection with CMGs thus:

$$\mathbf{D}_0 = \left[J_{W_{s1}} \hat{\mathbf{g}}_{\mathbf{s_1}} \;\; J_{W_{s2}} \hat{\mathbf{g}}_{\mathbf{s_2}} \;\; \ldots\ldots\ldots \;\; J_{W_{sN}} \hat{\mathbf{g}}_{\mathbf{s_N}} \right]_{3\times N} \tag{12a}$$

$$\begin{aligned} \boldsymbol{D} = [\ldots.(J_{s_i}\omega_{t_i} + (J_{g_i} - J_{t_i})\omega_{t_i})\hat{\boldsymbol{g}}_{s_i} \\ +(J_{s_i}\omega_{s_i} - (J_{t_i} + J_{g_i})\omega_{s_i} + J_{W_{si}}\Omega_i)\hat{\boldsymbol{g}}_{t_i}\ldots.]_{3\times N} \end{aligned} \tag{12b}$$

In 12b, the last term containing the wheel spin axis inertia and speed will have numerically significant value. This is because generally the wheel spin rates are at least 3000 times more than the spacecraft body rates. Combining the terms related to the CMG gyric torque, $\boldsymbol{L}_{gr}$ is defined as follows:

$$\boldsymbol{L}_{gr} = -\sum_{i=1}^{N} J_{W_{si}}\Omega_i(\omega_{g_i}\hat{\boldsymbol{g}}_{t_i} - \omega_{t_i}\hat{\boldsymbol{g}}_{g_i}) = \sum_{i=1}^{N}[\boldsymbol{\omega}^{\times}]\; J_{W_{si}}\Omega_i\,\hat{\boldsymbol{g}}_{s_i} \tag{13}$$

$\mathbf{L_{gr}}$ is the gyric torque acting on the spacecraft body due to coupling between the CMG angular momentum and spacecraft body rates. Though the formulation takes the same approach, the definitions of few terms ($\mathbf{D}$ and $\mathbf{L_{gr}}$) are different from the one given in [18]. In their work, Schaub et al.[18] consider a feedback control law along with the CMG states. However in this approach a cascaded saturation controller as explained in Sec. III.B will be used in the outer-loop for landmark acquisition and tracking. The definition of $\mathbf{D}_0$ is same as defined by [18]. However $\mathbf{D}$ and $\mathbf{L_{gr}}$ are different from [18] as the control laws discussed there are not used in the current application.

Following [17, 18] the terms related to gimbal acceleration ($\ddot{\boldsymbol{\gamma}}$) are ignored but the limits on the gimbal rates and accelerations will be imposed in the simulation. By substituting (12) and (13) in (11) results in the following equation which represents the combined dynamics of spacecraft with N-VSCMGs.

$$\boldsymbol{J}_{sat}\dot{\boldsymbol{\omega}} = -[\boldsymbol{\omega}^{\times}]\boldsymbol{J}_{sat}\,\boldsymbol{\omega} - \mathbf{D}_0\,\dot{\boldsymbol{\Omega}} - \mathbf{D}\,\dot{\boldsymbol{\gamma}} + \mathbf{L}_{gr} + \mathbf{L}_{ext} \tag{14}$$

where $\dot{\boldsymbol{\gamma}} = [\dot{\gamma}_1 \;\; \dot{\gamma}_2 \ldots\ldots\ldots \;\; \dot{\gamma}_N]^{\top}$ and $\dot{\boldsymbol{\Omega}} = [\dot{\Omega}_1 \;\; \dot{\Omega}_2 \ldots\ldots\ldots \;\; \dot{\Omega}_N]^{\top}$ are $\in \mathbb{R}^N$.

B. Acquisition and Tracking Attitude Controller

The acquisition and tracking controller is a composite nonlinear, multi-window controller with two saturation limiters and a PID at its core adopted from [21]. It incorporates two levels of saturation.

For rapid transient response, the inner saturation limit L_i is dynamically changed. It is defined as [21]; $L_i = \frac{c}{2k}\min\{\sqrt{4a_i|e_i|}, |\omega_i|_{max}\}$. Here, $|\omega_i|_{\max}$ is the specified maximum angular rate about the i^{th} axis; acceleration $a_i = T_{\max}/J_{\text{sat},ii}$ and T_{max} denotes the maximum torque output possible.

L_i is proportional to the maximum specified rate if the angular error is so large (as in the beginning of acquisition) that $\sqrt{4a_i|e_i|}$ exceeds the rate limit; here $|e_i|$ is a quaternion error, sine of a half angle error. Note that $\sqrt{4a_i|e_i|}$ is the maximum rate the spacecraft would acquire to render the quaternion error $|e_i|$ to zero with full torque. If the angular

error is not so large, then L_i is proportional to the lesser rate desired to bring the angle error to zero with full torque on. The L_i is converted to a quaternion error limit by its multiplication with $\frac{c}{2k}$.

The outer saturation is based on the maximum torque available from the CMGs using a normalized saturation function. The expression for computing the desired control torque using a PID compensator without the outer saturation is:

$$\boldsymbol{\tau} = -\boldsymbol{J}_{sat}\left(2k \underset{L_i}{\text{sat}}\left(\boldsymbol{e} + \frac{1}{T}\int \boldsymbol{e}\right) + c\,\boldsymbol{e}_{\boldsymbol{\omega}}\right) \tag{15}$$

where $\boldsymbol{e} = [q_{e1} \;\; q_{e2} \;\; q_{e3}]^\top$ is the quaternion error. The quaternion error is defined as the difference between the commanded and the current orientation as explained in [21] and $\boldsymbol{e}_{\boldsymbol{\omega}}$ is the error of the corresponding body rates.The gains k, c and T are proportional, derivative gains and T, the time constant of integral control are determined using the procedure explained in [21].

The final output after torque saturation is based on the formulation of the cascaded controller in [21].

$$\mathbf{L}_{c,des} = \begin{cases} \boldsymbol{\tau}, & \text{if } ||\boldsymbol{\tau}||_\infty < T_{max} \\ T_{sat}\frac{\boldsymbol{\tau}}{||\boldsymbol{\tau}||_\infty}, & \text{if } ||\boldsymbol{\tau}||_\infty \geq T_{max} \end{cases} \tag{16}$$

where $||\boldsymbol{\tau}||_\infty = \max(|\tau_x|, |\tau_y|, |\tau_z|)$. This desired value of the control torque $\mathbf{L}_{c,des}$ is added with $\mathbf{L}_{gr}$ to get the resultant commanded torque $\boldsymbol{L}_r$, which is equated with $\mathbf{D}_0\,\dot{\boldsymbol{\Omega}} + \mathbf{D}\,\dot{\boldsymbol{\gamma}}$ (17). $\boldsymbol{L}_r$ should be generated by the VSCMG/CMG cluster.

IV. VSCMG and CMG Steering Laws

A. VSCMG Steering Law

In (14), if we consider the sum of the second, third and fourth term on the RHS, $-\mathbf{D}_0\,\dot{\boldsymbol{\Omega}} - \mathbf{D}\,\dot{\boldsymbol{\gamma}} + \mathbf{L}_{gr}$, as the torque acting on the spacecraft denoted by $\boldsymbol{L}_c$ as shown in (17).

$$\begin{aligned} \boldsymbol{L}_c &= -\mathbf{D}_0\,\dot{\boldsymbol{\Omega}} - \boldsymbol{D}\dot{\boldsymbol{\gamma}} + \boldsymbol{L}_{gr} \\ \implies \mathbf{D}_0\,\dot{\boldsymbol{\Omega}} + \boldsymbol{D}\dot{\boldsymbol{\gamma}} &= -\boldsymbol{L}_{c,des} + \boldsymbol{L}_{gr} \triangleq \boldsymbol{L}_r \end{aligned} \tag{17}$$

The desired value of this torque, designated as $\boldsymbol{L}_{c,des}$ above, was calculated in Sec. III.B using a spacecraft attitude controller. For now, given the desired value of $\boldsymbol{L}_{c,des}$, a VSCMG steering law is invoked as follows.

Using the definitions given in [18], we define the Jacobian matrix of the N-VSCMG as $\mathbf{Q} = \begin{bmatrix}\mathbf{D}_0 & \mathbf{D}\end{bmatrix}_{3\times 2N}$. We also define state vector $\boldsymbol{\eta}$ in terms of the combined wheel acceleration and gimbal rate vector, $\dot{\boldsymbol{\eta}} = [\dot{\boldsymbol{\Omega}} \;\; \dot{\boldsymbol{\gamma}}]^T$. Using these definitions the VSCMG control law can be succinctly written as (18).

$$\mathbf{Q}\,\dot{\boldsymbol{\eta}} = \mathbf{L_r} \tag{18}$$

The variation in wheel speed for singularity avoidance need not be used always. The control law is designed in such a way that the output torque from wheels will be utilized only when the cluster is near a singular configuration. Following the treatment in [17, 18] a weighted pseudo-inverse steering law is used for VSCMGs as shown in (19) below.

$$\dot{\boldsymbol{\eta}} = \begin{bmatrix} \dot{\boldsymbol{\Omega}} \\ \dot{\boldsymbol{\gamma}} \end{bmatrix} = [W]\mathbf{Q}^T \left[\mathbf{Q}[W]\mathbf{Q}^T\right]^{-1} \mathbf{L_r} \tag{19}$$

If $[W] = I_{2N\times 2N}$, (19) reduces to the classical Moore-Penrose pseudo-inverse solution. Here, the weighing matrix $[W]$ is a diagonal positive definite matrix $[W] = diag\left\{W_{s_1}, W_{s_2}...W_{s_N}, W_{g_1}, W_{g_2}...W_{g_N}\right\}_{2N\times 2N}$.

The weights decide how active that particular CMG or RW will be. Making it zero will make the corresponding CMG/RW off. On the other hand, if it has a higher weight, then those RWs or CMGs will be more active in the generation of the output torque. The weights W_{g_i} ($i = 1$ to N) decides weight for output torque from CMGs.

The value of the weights $W_{s_i} = W_{s_i}^0\, e^{-\mu m}$, where $m = \sqrt{det\frac{1}{\bar{h}^2}\{\mathbf{D}\,\mathbf{D}^T\}}$ is the normalized singularity index of VSCMG. The assignment of the RW acceleration weights is different from that taken in [18], where the square root is absent. But the singularity avoidance laws for CMGs define the singularity index with the square root. Since this study plans to compare the VSCMG and CMG performance for completing the same manoeuvre, it was decided to retain the CMG definition of the singularity index here. However as can be seen in the results of the numerical simulations, the value of singularity index varies between 0 to 1.3 only and within this narrow range, the change in definition doesn't cause a significant difference in the steering law performance.

$W_{s_i}^0$ and μ are positive constants which are to be chosen appropriately depending on the problem. Since the VSCMGs have a time varying angular momentum, the singularity index is normalized by dividing it with a nominal value of the RW angular momentum $\bar{h}$. Whenever the CMG cluster approaches singularity, the singularity index becomes a small number. Consequently, the negative exponential term approaches 1 resulting in the utilization of the full weight $W_{s_i}^0$ for RW operation. In contrast, when the CMG gimbal configuration is away from singularity, the index m is relatively high, and the weight $e^{-\mu m}$ becomes small, and the cluster operates in the CMG mode.

The weighted pseudo-inverse steering law explained in 19 is the basic VSCMG steering law. However as explained in [18], by continuous addition of VSCMG null motion along with the torque generating rates, the control effort in the RW mode (i.e the RW output torque) can be minimized. This is critical in the point of view of reducing both the frequency of demanding high torque from RW motors and the overall power consumption. Thus a combination of VSCMG null motion steering laws are used with the torque generating rates.

Thus, three VSCMG steering laws are used in this study. The first one is mentioned in (19). The second steering law adds null motion to the torque generating steering law given in 19.

1. VSCMG Null Motion

The null motion uses a preferred gimbal angle and wheel speed as explained in [18] and given in (20).

$$\dot{\boldsymbol{\eta}}_{\boldsymbol{null}} = k_e \left(\hat{\mathbf{W}}\mathbf{Q}^{\mathbf{T}}[\mathbf{Q}\,\hat{\mathbf{W}}^{-\mathbf{1}}\,\mathbf{Q}^{\mathbf{T}}]^{-\mathbf{1}}\mathbf{Q} - \mathbf{I}_{\mathbf{2N}\times\mathbf{2N}} \right) \mathbf{A} \begin{bmatrix} \boldsymbol{\Delta\Omega} \\ \boldsymbol{\Delta\gamma} \end{bmatrix}_{2N\times 1} \tag{20}$$

Here, k_e, a scalar positive gain

$\hat{\mathbf{W}}$, the weighing matrix used in the null motion. Its numerical value will be different from that used in 19.

$\mathbf{I}_{2N\times 2N}$ is a $2N \times 2N$ identity matrix

$\mathbf{A}$, a diagonal matrix defined as shown in (21).

$$\mathbf{A} = \begin{bmatrix} a_{RW}[\mathbf{I}_{N\times N}] & [\mathbf{0}_{N\times N}] \\ [\mathbf{0}_{N\times N}] & a_{CMG}[\mathbf{I}_{N\times N}] \end{bmatrix} \tag{21}$$

a_{RW} and a_{CMG} can be set to 1 or 0. If either parameter are set to 0, this means that null motion will be performed without any preferred set of either $\boldsymbol{\Omega_f}$ and $\boldsymbol{\gamma_f}$. Also, $\boldsymbol{\Delta\Omega} = \boldsymbol{\Omega} - \boldsymbol{\Omega_f}$ and $\boldsymbol{\Delta\gamma} = \boldsymbol{\gamma} - \boldsymbol{\gamma_f}$ where $\boldsymbol{\Omega_f}, \boldsymbol{\gamma_f}$ are the preferred values for wheel speed and gimbal angles. Preferred gimbal angles (PGA) are those set of initial gimbal angles which configure the CMGs the farthest from internal singularities (refer to [14] for more details regarding the preferred gimbal angles). In this work, null motion is used to drive the cluster towards PGA as given in [15]. Thus the PGAs will have a high singularity index m (less singular geometry). The second steering law demands prior knowledge of the preferred gimbal angle derived through numerical simulation. If we want to overcome this a third steering law is introduced.

The third steering law is a variation in the null motion part where the variable $\boldsymbol{\Delta\gamma}$ is obtained from the gradient of the condition number, κ, of the CMG Jacobian matrix $\mathbf{D}$ as defined in (12b). It should also be noted that the unit vectors $\hat{\boldsymbol{g}}_s$ and $\hat{\boldsymbol{g}}_t$ within $\mathbf{D}$ will be time varying and have to be suitably considered in the gradient. A stiffer gimbal correction algorithm based on the gradient of the condition number κ is [18]:

$$\boldsymbol{\Delta\gamma} = k_g \left(1 - \kappa(t)\right) \frac{\partial \kappa}{\partial \boldsymbol{\gamma}} \tag{22}$$

where $\boldsymbol{\Delta\gamma}$ = the gimbal angle vector to be projected for the null motion in 22; k_g = a scale factor which scales the gradient step;$\kappa = \frac{\sigma_1}{\sigma_3}$ the ratio of the highest singular value to the lowest, of the Jacobian matrix $\mathbf{D}$ (refer [18], Sec. 8.8 for details of computing the gradient of κ). Ideally $\kappa = 1$ in the best case where the cluster is completely away from the singular configuration. While implementing, a dead-band κ_{db} is introduced such that whenever $\kappa \leq \kappa_{db} > 1$, the scalar $k_g = 0$ so that the null motion need not be executed.

B. CMG Steering Law: Singular Direction Avoidance (SDA)

The classical CMG equations can be obtained from the VSCMG dynamics by making the wheel acceleration term zero. Thus 17 simplifies to $\boldsymbol{D}\dot{\boldsymbol{\gamma}} = -\boldsymbol{L}_{c,des} + \boldsymbol{L}_{gr} \triangleq \boldsymbol{L}_r$. The inverse dynamics equations are solved by taking the pseudo-inverse of the Jacobian. The Jacobian is made invertible at singularity by addition of an error term. The SDA steering law introduced by Ford and Hall [12] is better than the pseudo-inverse. Unlike Singularity Roburst Inverse (SRI) or Generalized Singularity Robust Inverse (GSR) laws, which adds correction terms to all the singular directions, here the Jacobian matrix is rectified only about the most singular direction. This is achieved and implemented through the singular value decomposition (SVD) representation of the Jacobian matrix $\mathbf{D}$. Since the error term is added only to the most singular direction, the resultant torque error in a singular configuration will be less than the torque errors of other steering laws. The singular value decomposition of the Jacobian matrix is given as:

$$\mathbf{D}_{m\times n} = \mathbf{U}_{m\times m}\,\mathbf{S}_{m\times n}\,\mathbf{V^T}_{n\times n} \tag{23}$$

where $\mathbf{U}_{m\times m}$,$\mathbf{V}_{n\times n}$ are unitary matrices and $\mathbf{S}_{m\times n}$ a diagonal matrix. If $m \leq n$, then, the last $n-m$ columns of the $\mathbf{S}$ matrix will be zero. The SDA pseudo-inverse steering law is given as shown in (24).

$$\dot{\boldsymbol{\gamma}}_{SDA} = \mathbf{V_t}\,\mathbf{S}_{SDA}\,\mathbf{U^T}\,\mathbf{L_r} \tag{24}$$

where $\mathbf{V_t}$ is the truncated matrix obtained from $\mathbf{V}$ by eliminating the last $n-m$ zero columns and $\mathbf{S}_{SDA}$ is as defined below, after eliminating the last $n-m$ columns of the $\mathbf{S}$ matrix. S_{11}, S_{22} and S_{33} are singular values of the Jacobian matrix $\mathbf{D}$. The SDA correction factor α_{SDA}, is added only to the most singular direction S_{33}. The singular values appear as diagonal elements of the $\mathbf{S}$ matrix with $S_{11} \geq S_{22} \geq S_{33}$. Now after applying the SDA correction we obtain:

$$\mathbf{S}_{SDA} = \begin{Bmatrix} \frac{1}{S_{11}} & 0 & 0 \\ 0 & \frac{1}{S_{22}} & 0 \\ 0 & 0 & \frac{S_{33}}{S_{33}^2+\alpha_{SDA}} \end{Bmatrix} \tag{25}$$

We define $\sigma_{33} = \sqrt{\frac{3}{N}}\,\frac{S_{33}}{h}$, N = number of CMGs and h = individual wheel angular momentum (for one CMG) and $\alpha_{SDA} = \alpha_0\, e^{-k_\sigma\,\sigma_{33}^2}$ [12]. Here α_0 and k_σ are positive constants to be appropriately chosen depending on the problem at hand. Like other pseudo-inverse steering laws and their corrections, the SDA law can also encounters 'gimbal-lock'. This implies that at singularity, if $S_{33} = 0$, the steering law computes zero gimbal rate even for non-zero value of the commanded torque $\mathbf{L_r}$. Consequently the cluster remains trapped in a singular configuration. The addition of null motion along with the torque generating gimbal rate will help avoid this condition.

C. CMG Null Motion and Preferred Gimbal Angles

We define *null gimbal rates* $\dot{\boldsymbol{\gamma}}_{null}$ via the null space of $\boldsymbol{D}$ matrix, so that $\boldsymbol{D}\dot{\boldsymbol{\gamma}}_{null} = [0\,0\,0]^T$. It is evident that null rates change the gimbal angles of the CMG cluster without generating any output torque, and preserve the net angular momentum of the CMG cluster [5]. As such, null gimbal rates may be used to move the CMG cluster away from singularity without generating any output torque. A null projection matrix was defined in [5, 10] which will project any arbitrary $N \times 1$ vector $\mathbf{p}$ to the null space of the $\boldsymbol{D}$ matrix thus:

$$\dot{\boldsymbol{\gamma}}_{null} = [\boldsymbol{I_N} - \boldsymbol{D^T}(\boldsymbol{D}\,\boldsymbol{D^T})^{-1}\boldsymbol{D}]\ \mathbf{p} \tag{26}$$

Here $\mathbf{I_N}$ is an $N \times N$ identity matrix. Since the psuedoinverse of $\mathbf{D}$ is present within 26 as well, correction terms must be added here too for making it invertible under singular condition.

Vadali et al. define the Preferred Gimbal Angles (PGA) as a set of initial gimbal angles which is farthest from the internal singularity of the CMG cluster [14]. In addition, a CMG cluster when started from these initial conditions will traverse from zero angular momentum to the saturation angular momentum condition without encountering any internal singularities. This hasn't been proved for an arbitrary motion. Only a constant torque value about the body-axes with a 4-CMG pyramidal cluster was used to compute and analyze PGA in [14]. Nevertheless they can be used as a singularity free initial gimbal angle configuration for the CMG cluster. The PGAs are assigned at the beginning of the manoeuvre and it is not planned to bring the cluster back to PGA in between each targets, while performing multiple landmark acquisition and tracking.

In [15] the vector $\mathbf{p}$ is taken as the difference between a set of desired gimbal angles and current gimbal angles ($\mathbf{p} = \boldsymbol{\gamma}_{desired} - \boldsymbol{\gamma}$) to generate the null rates. In [14] a set of PGAs were taken as the desired gimbal angles ($\boldsymbol{\gamma}_{desired} = \boldsymbol{\gamma}_{pref}$). Here in the null motion expression, the null projection vector $\mathbf{p}$ is defined such that the corresponding gimbal rates drive the CMG cluster towards a set of preferred gimbal angles. The null rate using PGA are defined as:

$$\dot{\boldsymbol{\gamma}}_{null} = d\,[\boldsymbol{I_N} - \boldsymbol{D^T}(\boldsymbol{D}\,\boldsymbol{D^T} + \alpha\mathbf{I_3})^{-1}\boldsymbol{D}]\ (\boldsymbol{\gamma}_{pref} - \boldsymbol{\gamma}) \tag{27}$$

The term $\alpha\mathbf{I_3}$ is added to the $\mathbf{DD}^T$ term to aid its inversion at a singular gimbal angle configuration of CMG as explained in [14]. Two steering law combinations are used in case of CMG. The first case used the SDA law given in (24). The second case adds null motion as given in (27) with (24) with a suitable scale factor d. The null motion can be added more or less depending on the nearness of the cluster with a singular configuration. The null scaling can be taken of the form $d = d_0\, e^{-km^2}$ where d_0, k are positive constants and m is the singularity index (refer Sec.7.4 in [7]). In this way, null motion will be added more whenever the singularity index m is low (cluster is near singular) and vice-versa.

V. Numerical Simulations

In this section, multiple landmark acquisitions and tracking with 4-VSCMG and 4-CMG roof-type configurations (for roof-type cluster geometry refer[31]) are simulated, and their performances are illustrated and compared for the steering laws with and without null motion. The different cases considered are A) CMG Vs VSCMGs without null motion, B) VSCMGs with and without null motion, C) CMGs with and without null motion. Then best of the VSCMG steering laws is compared with the best of the CMG steering laws. For a fair comparison, the same set of targets is acquired with the same attitude controller for all cases. Their effectiveness and performance are compared for their ability to achieve the commanded torque, singularity index, pointing error, inertial tracking rate errors and gimbal rate. The VSCMG wheel speed variation and torque demanded are also studied to check their operating range and feasibility. A normalized torque error $\tau_{norm,e}$ defined as follows, is used to compare across steering laws.

$$\begin{aligned} \boldsymbol{\tau}_e &= \mathbf{L_r} - \mathbf{D}\dot{\boldsymbol{\gamma}}_{\boldsymbol{achvd}} \\ \tau_{norm,e} &= \frac{\|\boldsymbol{\tau}_e\|}{\sqrt{3}\,T_{max}} \end{aligned} \tag{28}$$

where $\dot{\boldsymbol{\gamma}}_{\boldsymbol{achvd}}$ is the achieved gimbal rate obtained from the computed gimbal rate, after rate limitation and by including the effect of gimbal dynamics (as a second-order transfer function), T_{max} is the maximum torque limit of the controller. Also, it may be worthwhile comparing the integral of the normalized torque error the total energy consumed across the steering laws. The parameters used for the numerical simulation are given in Table.1.

A. CMGs with SDA and VSCMGs without Null Motion

In this section a four-target multiple landmark acquisition and tracking manoeuvre is illustrated using a 4-CMG/VSCMG roof-type clusters. The CMGs are steered using the SDA law, (refer to (24), labeled "CMG:SDA" in Fig.2. The VSCMGs use the steering law (refer to 19), which weighs the utilization of the CMGs spinning wheels as reaction wheels near singularity. Performance of the VSCMGs is identified as "VSCMG" in Fig.2 and subsequently both these laws are illustrated without a null motion.

Fig.2 shows the demanded torque by the controller and what is produced by the CMG and VSCMG clusters about the x,y and z axes. Each target is allocated 35 seconds for both acquisition and tracking (Table.1). Each positive and negative torque pulse represents a high-torque acquisition phase followed by a low-torque settling and tracking phase. Both steering laws entail errors in the achieved torque. The normalized torque errors for both CMGs and VSCMGs and target flags at t = 35, 70, 105 s are shown in Fig.3. Large error at the start of target acquisition may be ignored as it occurs due to the instantaneous torque demanded by the controller. By examining the torque errors for each target, one can observe that except for high torque error $\tau_{norm,e} = 0.6$ at t = 54s for CMG:SDA law, the error VSCMGs entail is high considering all the four targets.

Table 1 Parameters used for Landmark Acquisition and Tracking Using CMGs and VSCMGs

Parameter	Value
Time per target	35 s
Initial Euler Angle	$[0\,10\,0]^T deg$
Inertia Matrix	diag (1200 1300 1100) $kg.m^2$
Orbital Period	94 min
Altitude	450 km
PID gains: c,k,T	5.78 rad-s,11.3 rad-s^2, 2.5s
Max rate: Roll,Pitch, Yaw	[4,3,2] deg/s
Max accel: Roll,Pitch,Yaw	0.6 deg/s^2
T_{max}-Roll,Pitch,Yaw	13.6 N.m
Acce limit factor: λ_{lim}	0.5
Initial Gimbal angle,$\boldsymbol{\gamma}(t_0)$	$[45^\circ\ -45^\circ\ \ 45^\circ\ -45^\circ]^T$ deg
Preferred Gimbal Angle, $\boldsymbol{\gamma}_{pref}$,$\boldsymbol{\gamma}_f$	$[45^\circ\ -45^\circ\ \ 45^\circ\ -45^\circ]^T$ deg
Wheel Speed, $\boldsymbol{\Omega}_(t_0)$	$[3250\ 3250\ -3250\ -3250]^T$ rpm
Preferred Wheel Speed, $\boldsymbol{\Omega}_f$	$[3250\ 3250\ -3250\ -3250]^T$ rpm
Skew Angle of cluster, β	30 deg
Nominal wheel angular momentum, h	25 N.m.s
Maximum gimbal rate limit, $\dot{\gamma}_{max}$	45.8 deg/s
Max. CMG Output Torque	20 N.m
Max. RW Output Torque	0.25 N.m
VSCMG: Wheel weight	$0.5\,e^{-5m}$
VSCMG: Null Motion weight	$1.0\,e^{-5m}$
VSCMG: Null motion gain,k_e	0.25 (VSCMG:Null 1), 5×10^{-4} (VSCMG:Null 2)
VSCMG: Scale factor for gradient, k_g	0.5 (VSCMG:Null 2)
CMG, α_{SDA}	$0.5\,e^{-10\sigma_{33}^2}$
CMG Null Motion, d	$0.75\,e^{-10\,m^2}$
Number of Targets	4
Integration time step	0.01 s

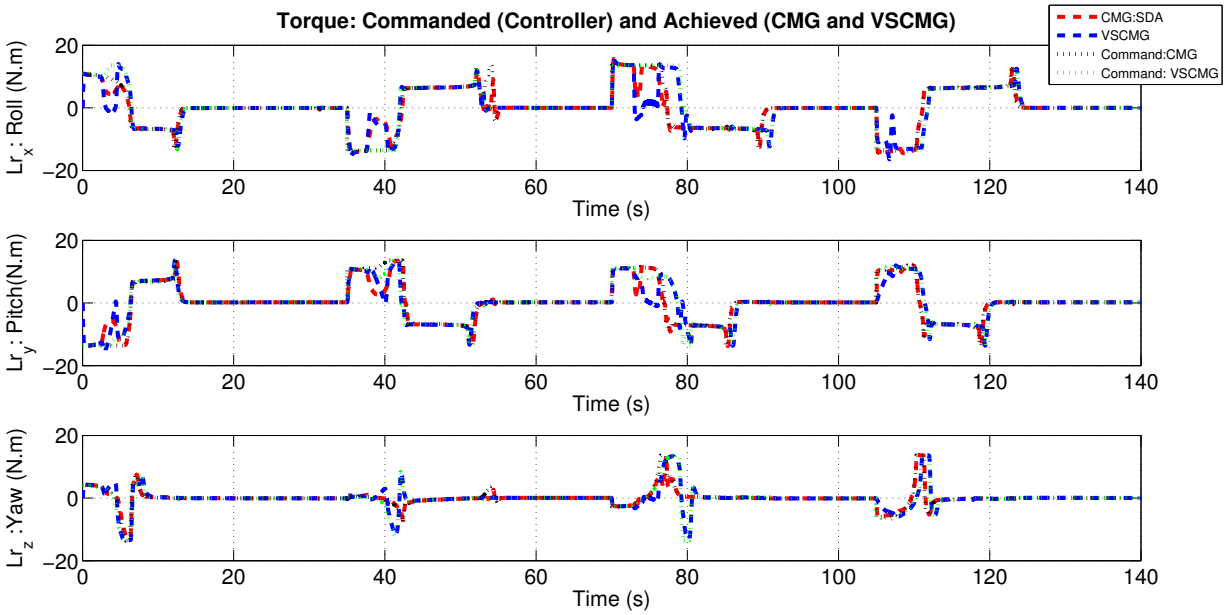

Fig. 2 Commanded and Achieved torques using 4-CMG and VSCMG cluster. Standalone steering law without null motion for all four targets

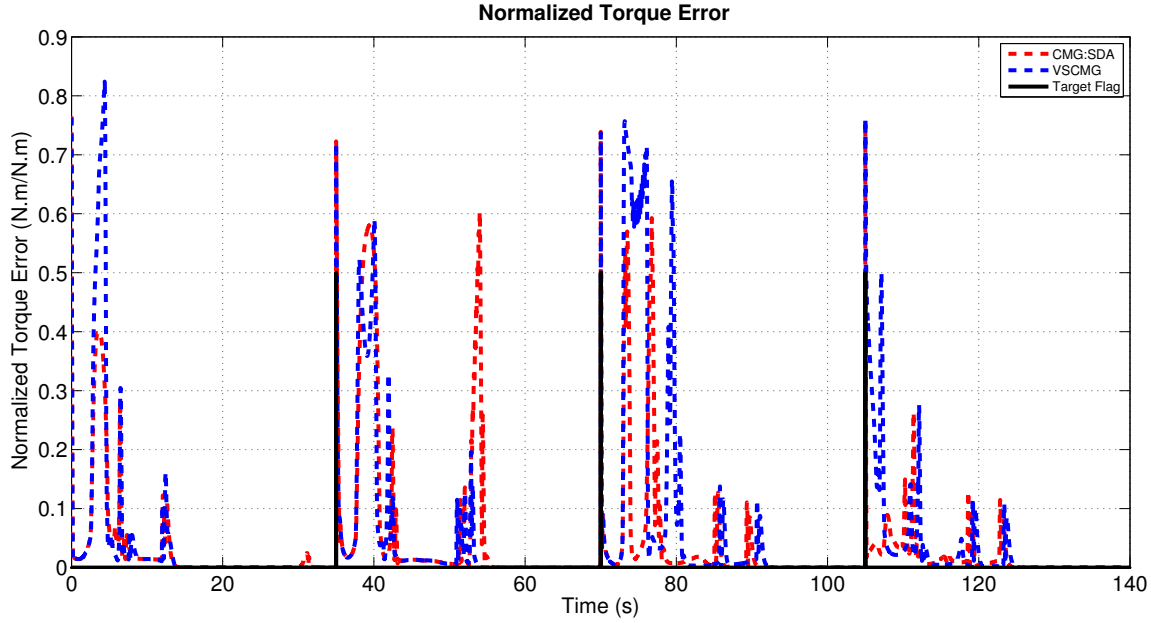

Fig. 3 Normalized torque error using 4-CMG and VSCMG cluster. Standalone steering law without null motion for all four targets.

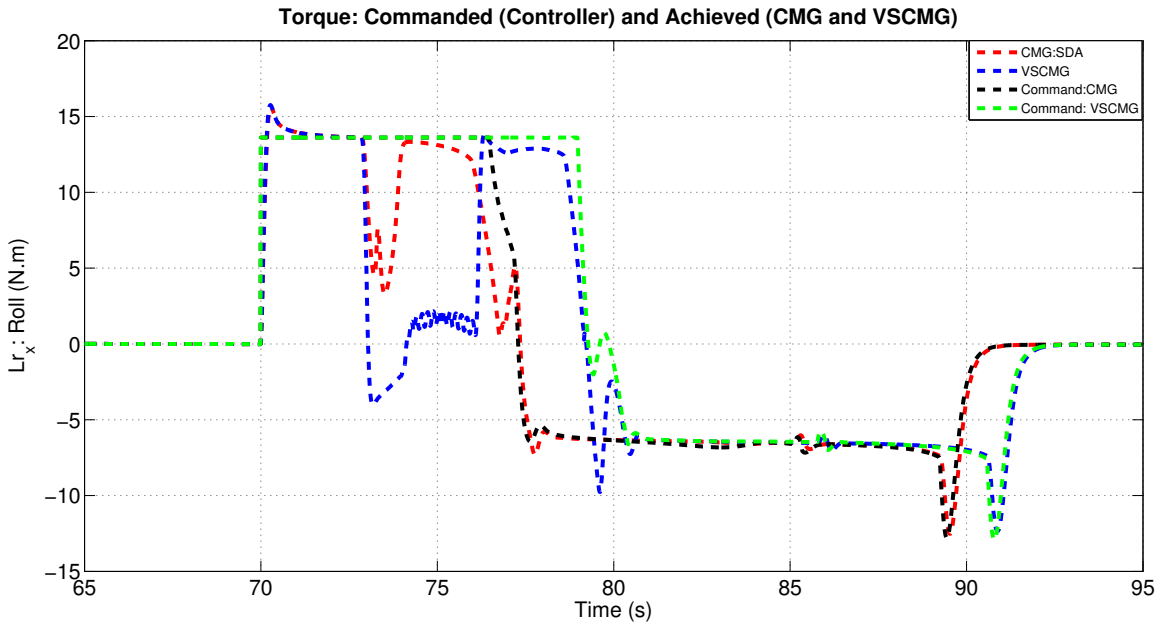

Fig. 4 Commanded and Achieved torques using 4-CMG and VSCMG cluster. Standalone steering law without null motion. Torque about the x-axis is enlarged while acquiring and tracking target 3

For greater clarity, the x-axis torque for acquiring and tracking target-3 is enlarged and shown in Fig.4. Here we observe that the CMG:SDA law is able to better track the commanded torque and it deviates lesser than the VSCMGs do. It also shows reduced oscillations when compared to VSCMGs. Between t = 73s to t = 77s, at the point of largest torque error, VSCMG gives a torque output of -4.0 N.m to 1.2 N.m against a demanded torque of 13.6 N.m. The corresponding values for CMG:SDA law are 3.3 N.m and 0.96 N.m for a mere 1.1 s against 3.5 s for the VSCMGs. Consequently, the CMG:SDA law switches to the tracking phase at t = 91.1 s whereas the VSCMGs do about a second later at t = 92.4 s. This is illustrated below in the pointing error plots (Fig.6 and Fig.7).

The singularity indexes m of the two steering laws under study is shown in Fig.5. For both CMGs and VSCMGs, the m index is defined as, $m = \sqrt{det\frac{1}{h^2}\{\mathbf{D}\,\mathbf{D}^T\}}$. This is because the VSCMG action, by varying the speed of the RW, is also exercised based on the drop in CMG m index. The singularity index for CMG:SDA is nearly zero at t=30.9s, 53.8s, 73.3s and 76.8s. The largest torque error is caused by the singularity at t=53.8s as shown in the normalized torque error plot (refer Fig.(3)). These torque errors occur for short 2-3 seconds. For the VSCMG cluster, low index was seen at t=52.8 s, 73s-76s (with oscillations) and 79s. The drop in singularity index seen between 73s-76s can be correlated with the large torque error seen during this period while acquiring target-3.

The comparison of attitude errors with CMG:SDA and VSCMG steering laws (refer to Fig.6-Fig.7) is given in Table.2. Here the peak value of the normalized torque error ($\tau_{e,norm} : max$) and the time instants at which the pointing and rate errors become less than the thresholds of $0.005°$ (t_E) and $0.001°/s$ (t_ω), respectively, are given. The payload operation commences at time t_P when both errors are below thresholds. The commencement time difference between

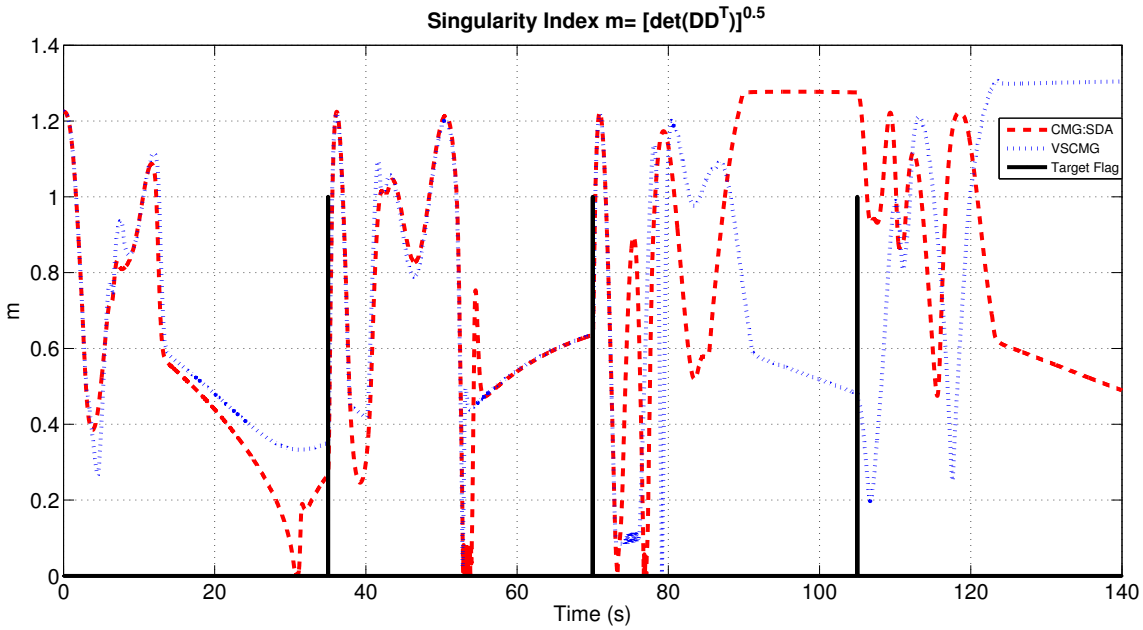

Fig. 5 Singularity Index m of standalone steering law without null motion for 4-CMG and VSCMG cluster.

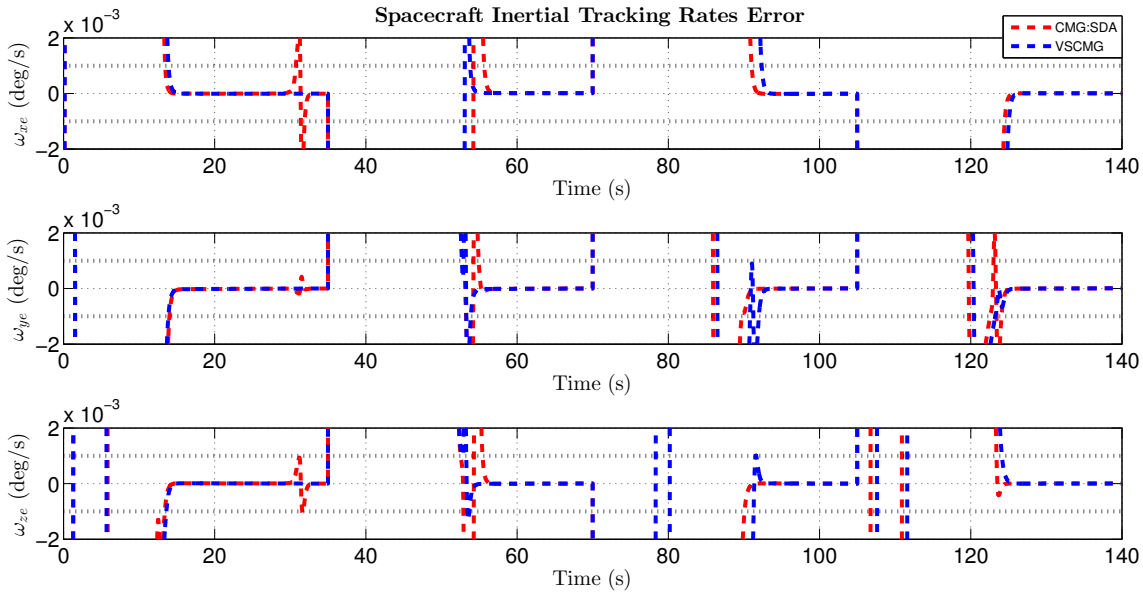

Fig. 6 Inertial tracking rate error of CMG:SDA and VSCMG steering laws without null motion. Error threshold demanded during tracking is $0.001°/s$ (black dotted line)

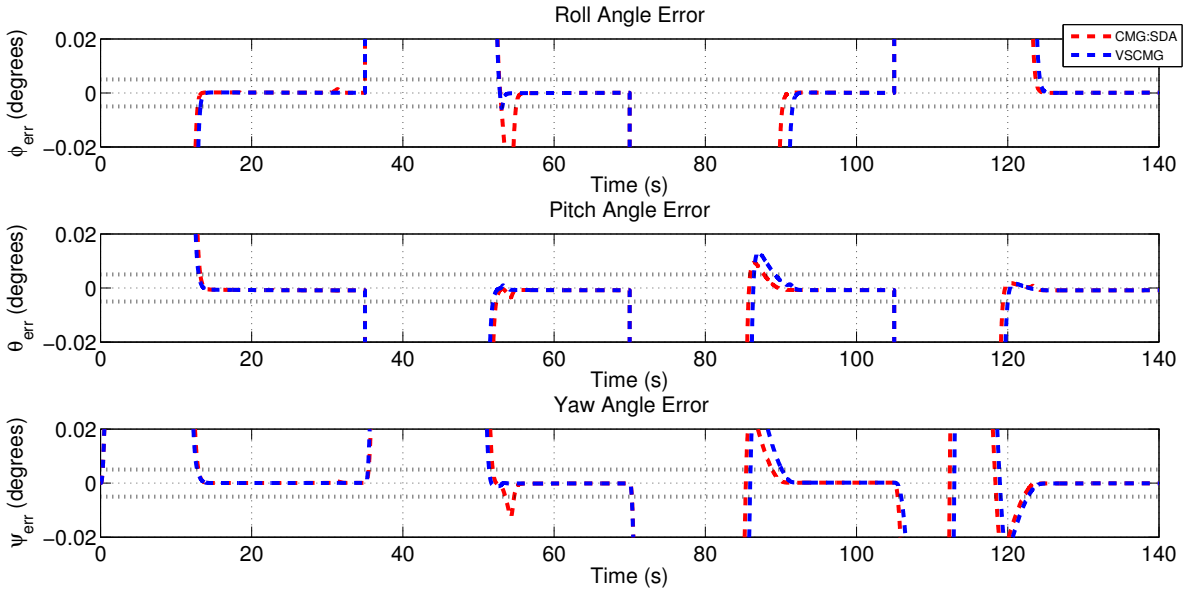

Fig. 7 Pointing error of CMG:SDA and VSCMG steering laws without null motion. Pointing error threshold specification is 0.005° **(black dotted line)**

t_P of VSCMG and CMG:SDA steering laws is denoted by Δt. Here a positive value means that the target acquisition period of the CMG:SDA is shorter than that of the VSCMGs, and the CMG:SDA begins target tracking and surveillance sooner than the VSCMGs. For target 1, both CMG:SDA and VSCMGs commence the target tracking at 14s, but at t = 30.9 s the CMG:SDA tracking rate error exceeds the threshold for 1.2 s due to singularity, as shown in Fig.6. For target 2, the VSCMGs commence payload operation 1.78 s sooner than the CMG:SDA does. For target 3 and 4, the CMG:SDA law is faster by 1.33 s and 0.5 s respectively.

Table 2 Comparison of CMG:SDA and VSCMG steering laws while acquiring and tracking four targets

Performance of CMG:SDA and VSCMG						
Parameters		$\tau_{e,norm}$: max	t_E (s)	t_ω (s)	t_P (s)	Δt (s)
Target-1	**CMG:SDA**	0.4	13.2	14.00	14.00	-1.3*
	VSCMG	0.81	13.2	13.9	13.9	
Target-2	**CMG:SDA**	0.6	54.98	55.66	55.66	-1.78
	VSCMG	0.60	53.16	53.88	53.88	
Target-3	**CMG:SDA**	0.53	90.23	91.02	91.02	1.33
	VSCMG	0.76	91.56	92.35	92.35	
Target-4	**CMG:SDA**	0.26	123.7	124.5	124.5	0.50
	VSCMG	0.71	124.3	125.1	125.1	

**CMG:SDA Law goes out of tracking rate threshold for 1.2 seconds from t = 30.7 s and 31.9s.*

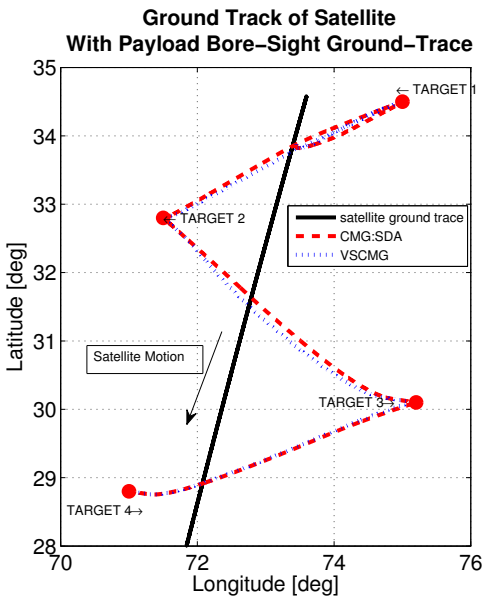

Fig. 8 Achieved payload bore-sight and satellite ground trace with CMG:SDA and VSCMG steering laws without null motion.

The sub-satellite point and payload bore-sight ground traces along with the four targets as acquired by the CMG:SDA and VSCMG steering laws are shown in Fig.8. The targets are on both sides of the satellite ground trace. The CMG/VSCMG clusters steer the body mounted payload from one target to the next as the satellite traverses as shown.

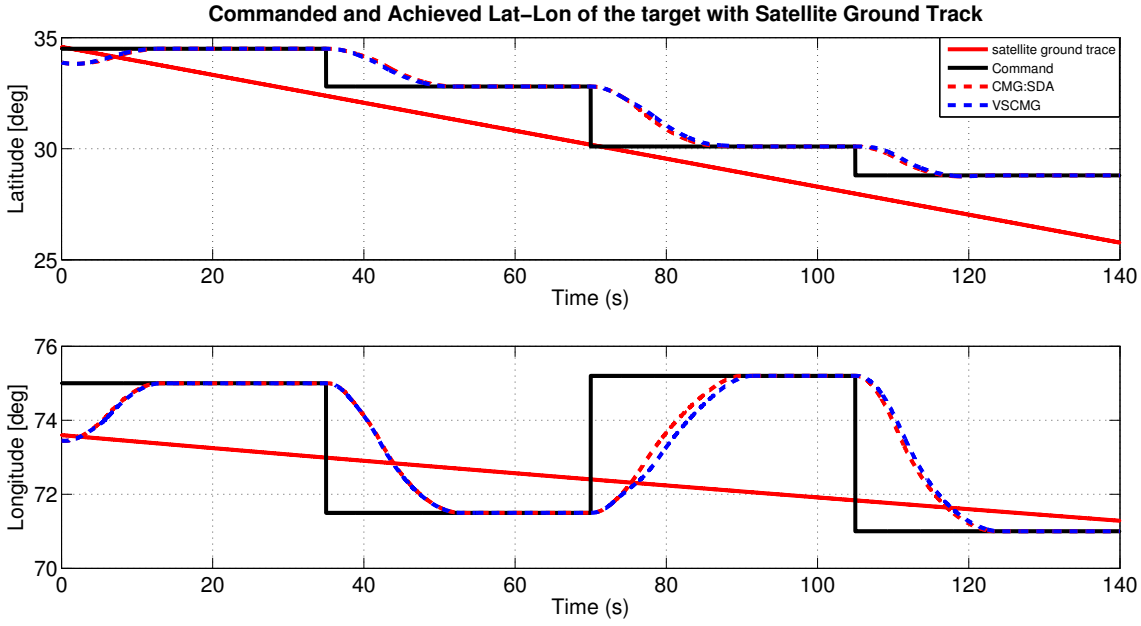

Fig. 9 Commanded and achieved latitude and longitude values of the targets with CMG:SDA and VSCMG steering laws without null motion. The spacecraft ground trace (solid red line) is also shown

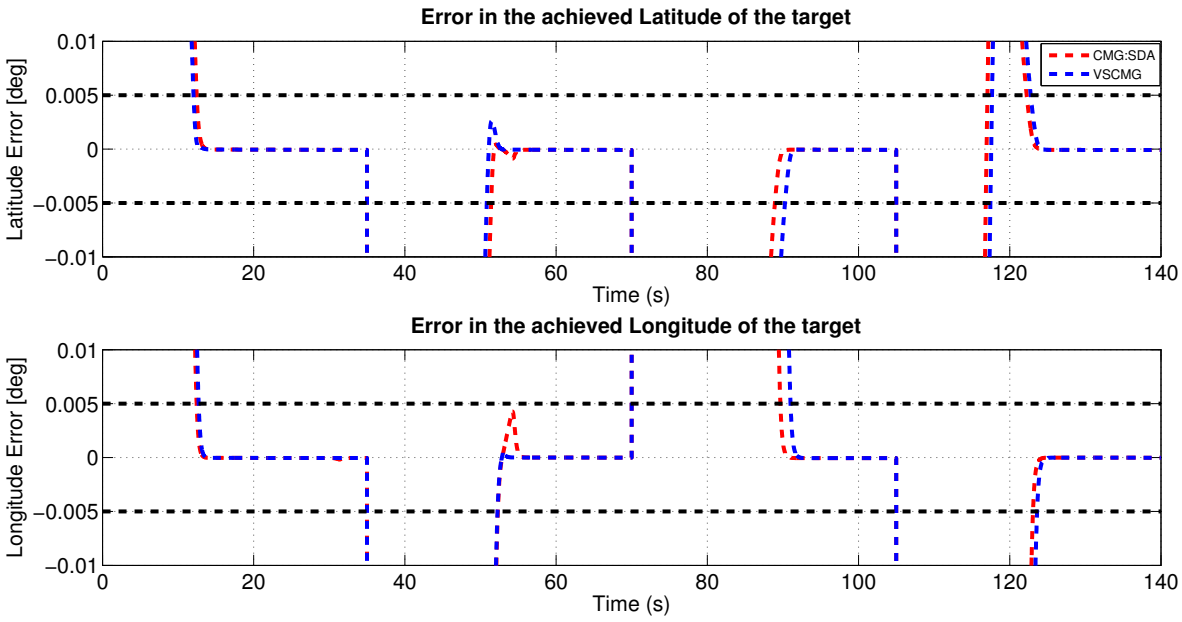

Fig. 10 Error in achieved latitude and longitude values of the targets with CMG:SDA and VSCMG steering laws without null motion.

In order to understand the acquisition process better, the instantaneous latitude and longitude of the payload bore-sight, for the realized in-track and cross-track angles and the commanded constant latitude and longitude of the four targets on the rotating earth are shown in Fig.9. The satellite ground trace lat-lon is also shown. The payload bore-sight is initially pointed elsewhere from where it is manoeuvred to reach the desired target of interest. This is a large angle manoeuvre and demands the full torque capability of the CMG cluster. From the commanded and achieved latitudes and longitudes, performance of CMG:SDA law is better than VSCMG law for target 3 and 4.

Further insight can be obtained from the latitude and longitude errors shown in Fig.10. This is similar to the pointing errors shown in Fig.7. The effect of inertial tracking rate error can not be captured in this figure. However, this is a critical factor desired for final payload operation. The latest time taken for both latitude and longitude to reach within the desired error threshold is noted. They are similar for targets 1 and 2. For targets 3 and 4 the CMG:SDA laws is faster by 0.5 to 1.3 seconds. However the time taken for the tracking rate error to fall within the threshold is always longer than that required for achieving the pointing error in all cases (refer Table.2) and is the dominant factor in deciding the final payload operation time.

The gimbal rate histories for the two steering algorithms are given in Fig.11. The maximum gimbal rate is limited to $45.8^{\circ}/s$. However one can observe the oscillations in gimbal rate near t=53.8 s for the CMG:SDA law and near t=75.31s for the VSCMG law corresponding to the oscillations seen in the singularity index (refer to Fig.5). It is not desirable to have oscillations in gimbal rate during CMG operation as it will impart undesirable disturbances to the platform during gimbal motor operation.

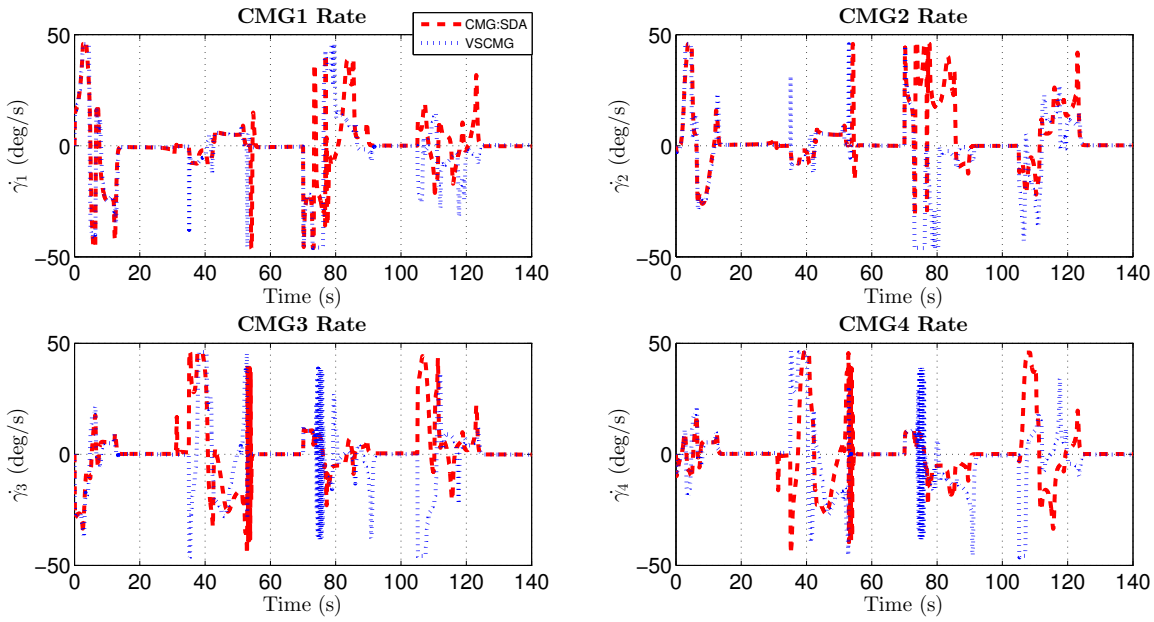

Fig. 11 Gimbal rate history of standalone steering law without null motion for 4-CMG and 4-VSCMG cluster.

B. VSCMG Based Manoeuvre: With Null Motion

In the previous sub-section, CMGs with singular direction avoidance Vs VSCMG steering law, both without null motion were studied. In this sub-section, the effect of null motion in improving the VSCMG performance is explored. Two types of null motions are considered. The first law, as explained in 20, is used to achieve the nominal spin speed and preferred gimbal angles; denoted as 'VSCMG:Null 1' below. The second law, uses null motion to avoid singularity using the gradient of the condition number (22); denoted as 'VSCMG:Null 2' below. These are added with the torque generating rates (19). The VSCMG steering law; denoted as 'VSCMG' is also given for illustrating the improvement in VSCMG performance by the addition of null motion.

The commanded and achieved torques about the three body axes are shown in Fig.12. As it can be observed, there are differences between the demanded and achieved torque whenever peak torque is asked by the controller. However, how well the commanded torque is achieved varies from one VSCMG steering law to another.

The normalized torque error for the three steering laws with target flag is given in Fig.13. For the first two targets, the normalized torque error shows a very small difference across the steering laws. For target 3, the peak value of torque error for VSCMG:Null 1 ($\tau_{e,norm}$ = 0.84) is greater than those of other two laws ($\tau_{e,norm}$ = 0.76). However, the former occurs for less than 2 s whereas the latter two for 5 s each. The number of peaks are fewer for VSCMG:Null 1. For target 4, the three laws show a clear distinction with VSCMG:Null 1 giving the lowest torque error, followed by VSCMG law without null motion and VSCMG:Null 2.

The x-axis torque demanded by the controller and that obtained by VSCMG, VSCMG:Null 1 and VSCMG:Null 2

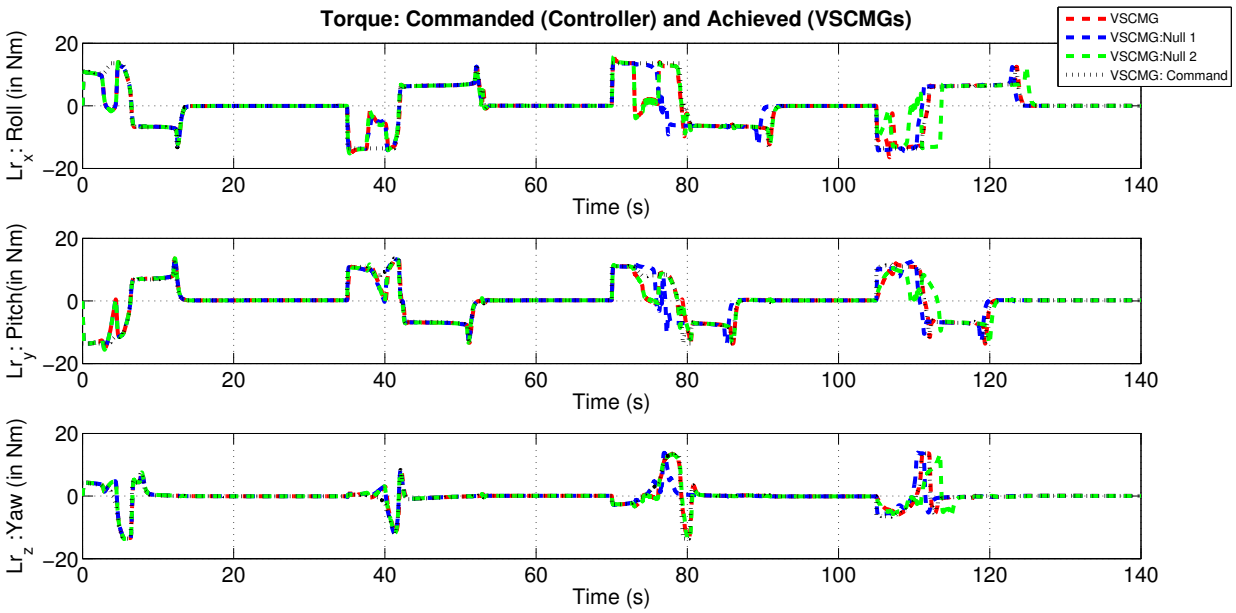

Fig. 12 Commanded and Achieved torques using 4-VSCMG cluster with and without null motion for all four targets

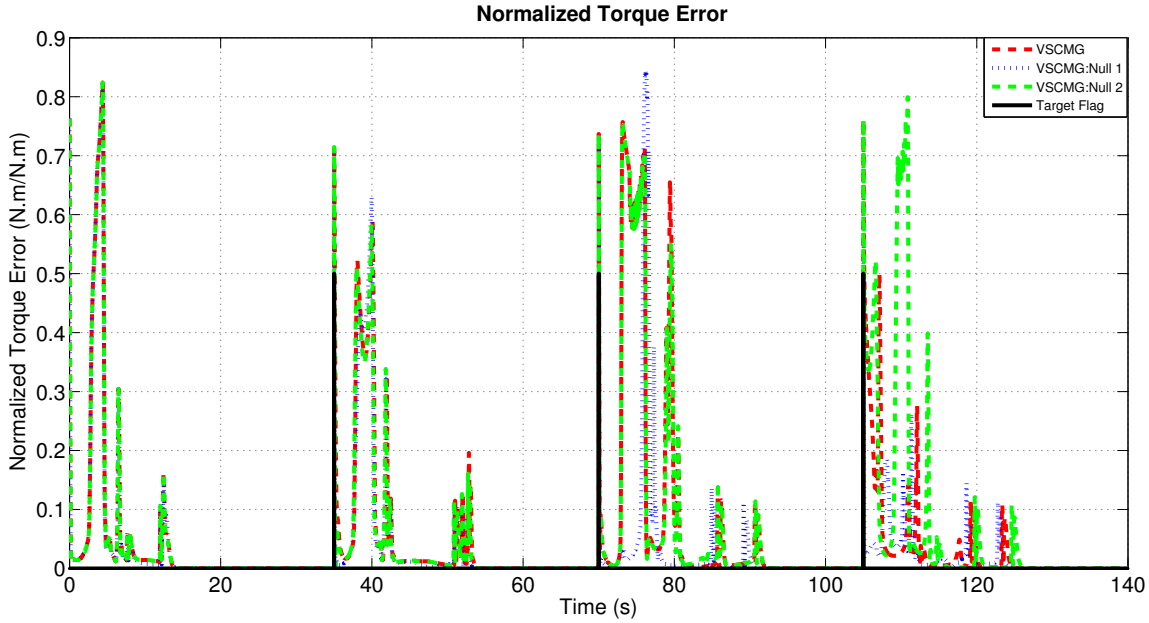

Fig. 13 Normalized torque error using 4-VSCMG cluster with and without null motion for all four targets.

while acquiring and tracking target 4 are enlarged and given in Fig.14. The demanded torque from the controller also varies depending on the error in the achieved torque. So, compared to Fig.12 , Fig.14 shows the additional variables Command-VSCMG:Null 1 and Command-VSCMG:Null 2.

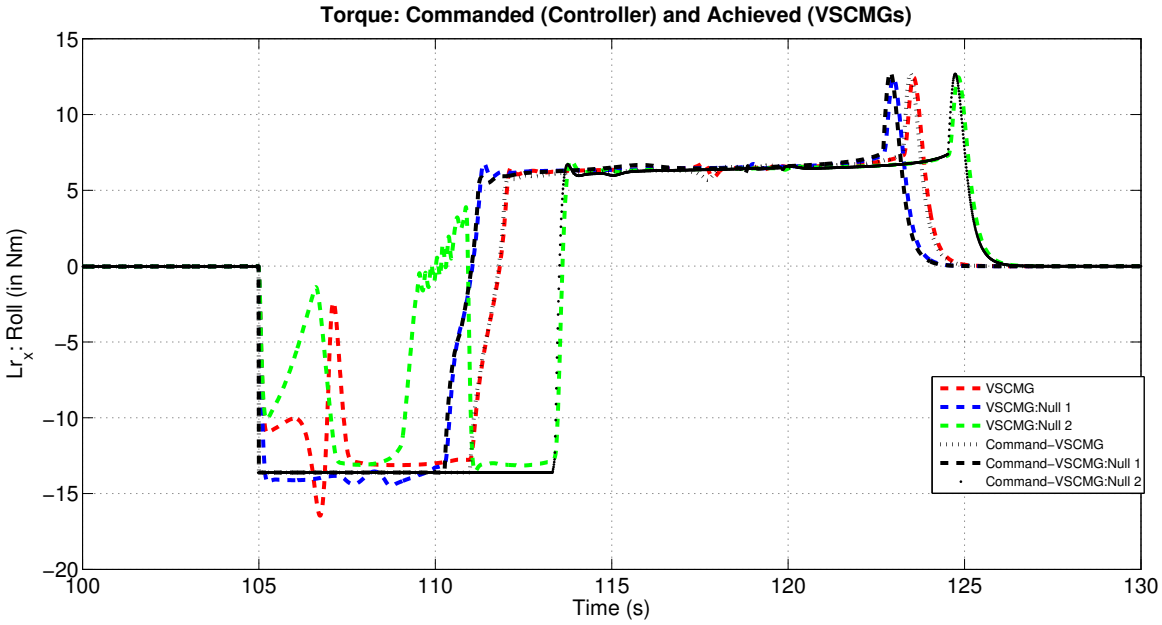

Fig. 14 Commanded and Achieved torques 4-VSCMG cluster with and without null motion. Torque about the x-axis is enlarged while acquiring and tracking target 4

Let us consider first the VSCMG: Null 2 Steering law (that is, the VSCMG steering law with null motion based on the gradient of κ). There are two large dips in the achieved torque (-2.1 N.m and -1.6 N.m against a demanded torque of -13.6 N.m) and torque oscillations between t=105 s to t=112 s. The VSCMG steering law without null motion also entails torque error as seen by the torque dip of -2.7 N.m against a demand of -13.6 N.m at t=107 s. One can observe that the VSCMG: Null 1 (a combination of (19) and (20), using the preferred gimbal angle and nominal spin speed) is able to faithfully track the demanded torque with least deviation. Better torque tracking prevails when the torque polarity changes and the torque magnitude decreases (from -13.6 Nm to 6.4 Nm) for all laws. Consistent with their torque error, the VSCMG:Null 1 law completes deceleration and enters the tracking phase first, followed by VSCMG and then by VSCMG:Null 2.

The singularity indexes for the three steering laws are shown in Fig.15. The m index for the VSCMG is computed from the **D** matrix, without considering the wheel acceleration terms. Since the major portion of the generated torque is obtained from CMGs, the singularity index directly influences the torque error. The dips seen earlier, in the achieved torque are correlated with the corresponding drop in the singularity index m. The m indexes of the steering laws vary together till t = 11.6 seconds after which the three diverge. The VSCMG:Null 2 varies almost similar to the VSCMG law. Between t = 90 s to t = 105s, the VSCMG: Null 2 law gives a higher m index than VSCMG law. However, the

VSCMG: Null 2 law reaches very low values ($m = 0.05$) between $t = 109.5$s and $t = 111.5$s. The index m for the VSCMG:Null 1 behaves similarly but only for 0.5 s near 76 s.

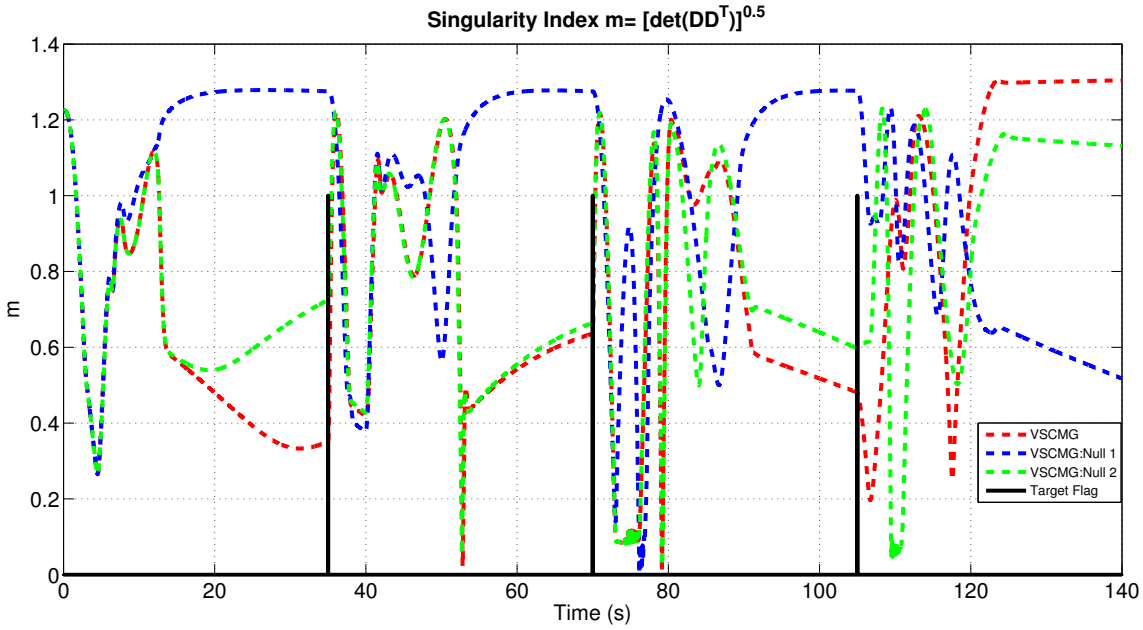

Fig. 15 Singularity Index m of with and without null motion for 4-VSCMG cluster.

Fig.16 shows the residual inertial tracking rate error while Fig.17 shows the corresponding pointing errors in roll,pitch and yaw using the three VSCMG steering laws. Similar to the observation seen earlier, the tracking performance is comparable for the first two targets while for the last two the VSCMG:Null 1 gives superior performance. The peak normalized torque error and the time taken by the three steering laws to reach within the angle and rate threshold for four targets are listed in Table.3. The last column of Δt represents the time difference between t_P of VSCMG:Null 1 and the longer t_P between the VSCMG: null 2 and no null motion steering laws. For target 1, VSCMG:Null 1 is slower by 0.2 s while it is 1.5 s and 1.8 s faster for the targets 3 and 4, respectively.

The ground traces of the payload bore-sight with the three steering laws is shown in Fig.18. Similar to the results seen in Table.3, the three ground traces from target 1 and target 2 are overlaid. The latitude and longitude errors in arriving at the target are portrayed in Fig.19. The performance of the three steering laws is the same for targets-1,2. For target-3,4 VSCMG:Null 1 steering law performs better.

The gimbal rates are shown in Fig.20. The computed gimbal rate magnitudes are limited to $45.8^\circ/s$ and are hence feasible. However, corresponding to the oscillations seen in the singularity index (refer to Fig.15) seen at t=75 s ($m = 0.1$) for both VSCMG and VSCMG:Null 2, the oscillations are observed in the gimbal rates (variation between $38^\circ/s$ to $-38^\circ/s$ with a time period of 0.3 s in Fig.20) for CMG-3 and CMG-4. The oscillations occur again for the VSCMG:Null 2 at $t = 110$s. This doesn't happen in case of VSCMG:Null 1 law. The oscillations are undesirable as

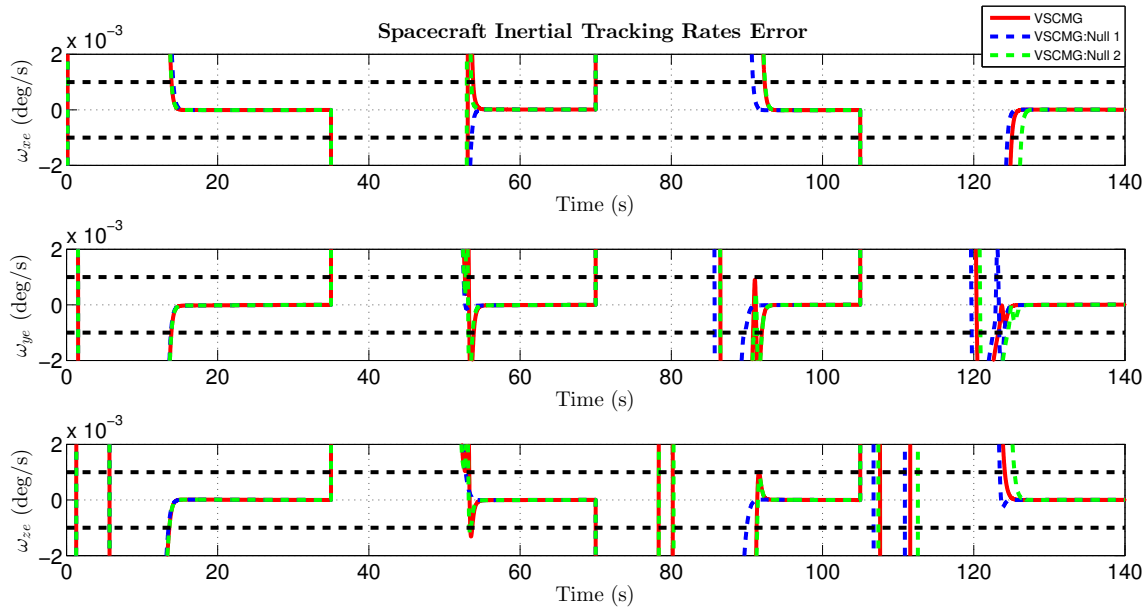

Fig. 16 Inertial tracking rate error with and without null motion for 4-VSCMG cluster. Error threshold demanded during tracking is $0.001°/s$ (black dotted line)

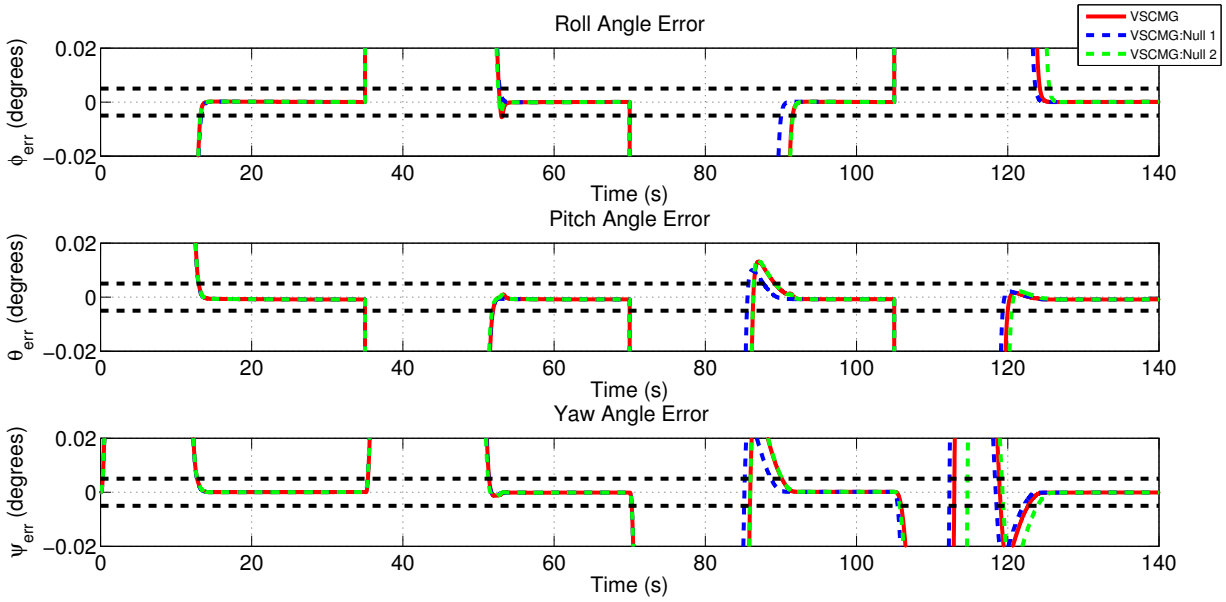

Fig. 17 Euler angle error with and without null motion for 4-VSCMG cluster. Error threshold demanded during tracking is $0.005°$ (black dotted line)

Table 3 Comparison of VSCMG steering laws with and without null motion while acquiring and tracking four targets

Performance of VSCMG Laws: With and Without Null Motion						
Parameters		$\tau_{e,norm} : max$	t_E (s)	t_ω (s)	t_P (s)	Δt (s)
Target 1	**VSCMG**	0.82	13.2	13.9	13.9	-0.2
	VSCMG:Null 1	0.82	13.3	14.1	14.1	
	VSCMG:Null 2	0.82	13.2	13.9	13.9	
Target 2	**VSCMG**	0.58	52.6	53.7	53.7	0
	VSCMG:Null 1	0.63	52.8	53.7	53.7	
	VSCMG:Null 2	0.58	52.6	53.7	53.7	
Target 3	**VSCMG**	0.76	91.5	92.3	92.3	1.5
	VSCMG:Null 1	0.84	90.1	90.8	90.8	
	VSCMG:Null 2	0.76	91.5	92.3	92.3	
Target 4	**VSCMG**	0.50	124.3	125.1	125.1	1.8
	VSCMG:Null 1	0.26	123.7	124.5	124.5	
	VSCMG:Null 2	0.80	125.5	126.3	126.3	

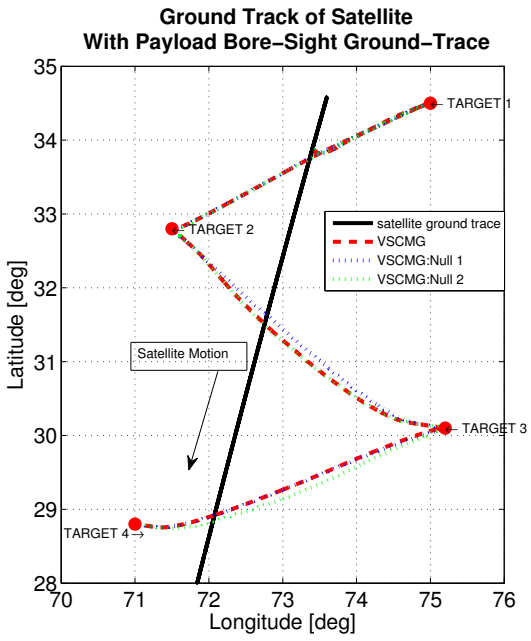

Fig. 18 Achieved payload bore-sight and satellite ground trace with standalone steering law without null motion for 4-CMG and VSCMG cluster.

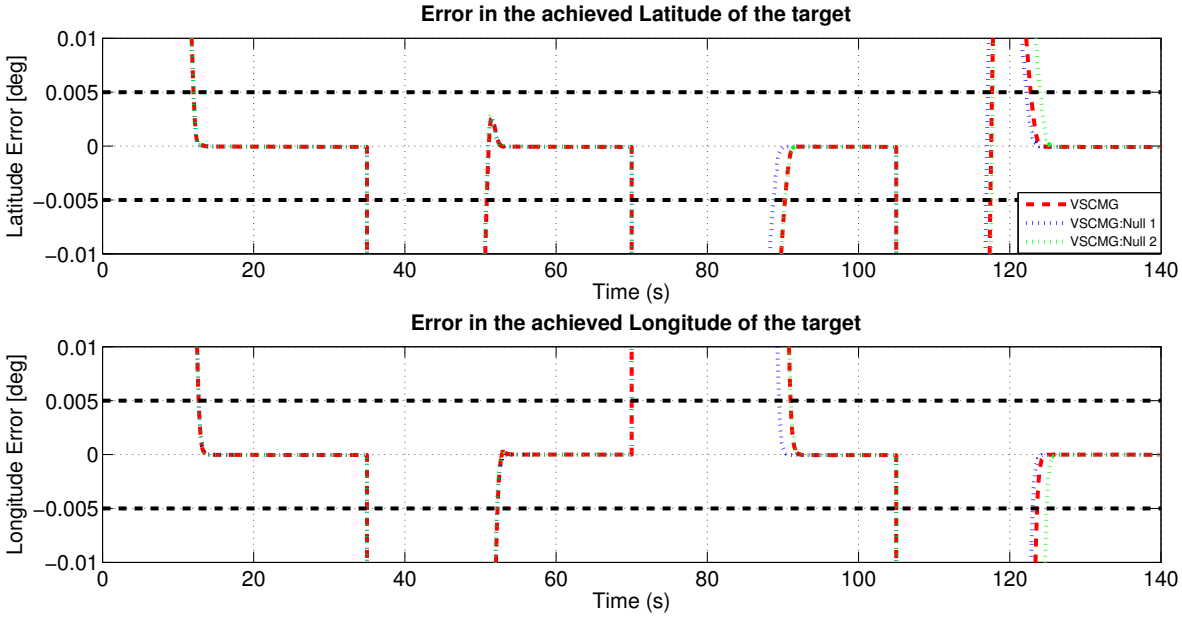

Fig. 19 Error in achieved latitude and longitude for 4-VSCMG cluster. Error threshold demanded during tracking is 0.005° **(black dotted line)**

that would entail high gimbal accelerations from the gimbal motor, and thereby resulting in unwanted disturbance on the platform.

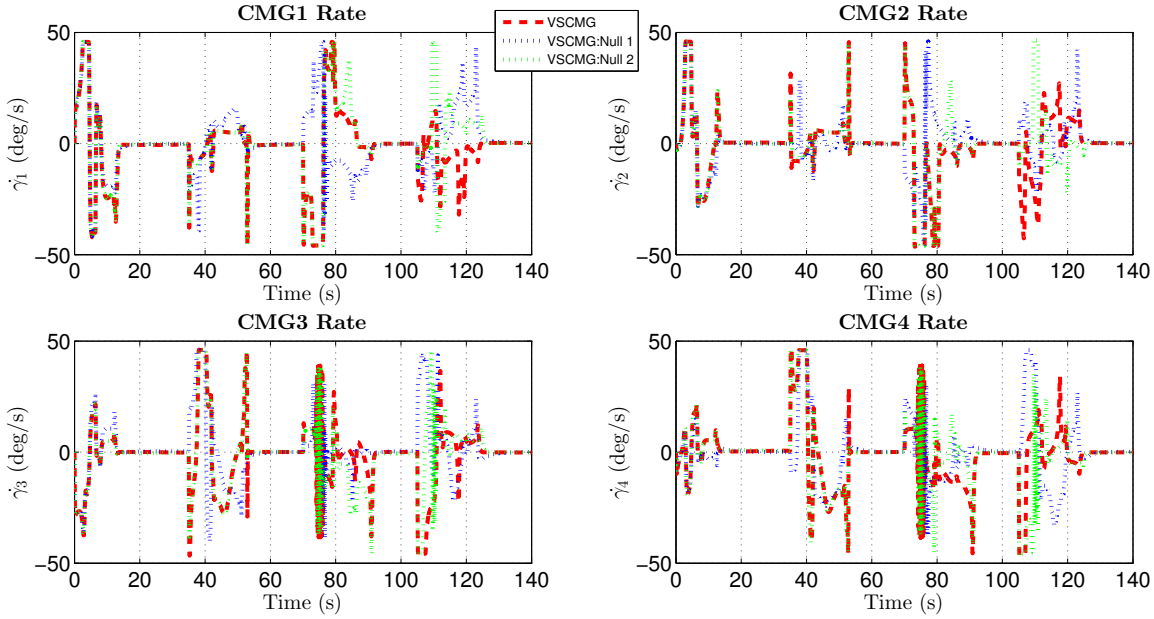

Fig. 20 Gimbal rate history with and without null motion for 4-VSCMG cluster.

The variation in wheel speed and wheel motor torque are shown in Fig.21 and Fig.22. The maintenance of wheel

speed to the initial value was used in both forms of null motion law. In VSCMG: Null 2 law, the gimbal angles alone are chosen from the gradient of the condition number. Recall that in VSCMG: Null 1, these were chosen as the preferred gimbal angles. The wheel speed variation is the highest for the VSCMG: Null 2 law, followed by VSCMG. The VSCMG:Null 1 law has the lowest variation as it maintains a better singularity index than the other laws. So it demands lesser wheel speed variations to overcome singularity. The maximum wheel torque values computed are limited within 0.25 N.m, which is feasible with existing wheel designs without any major modifications.

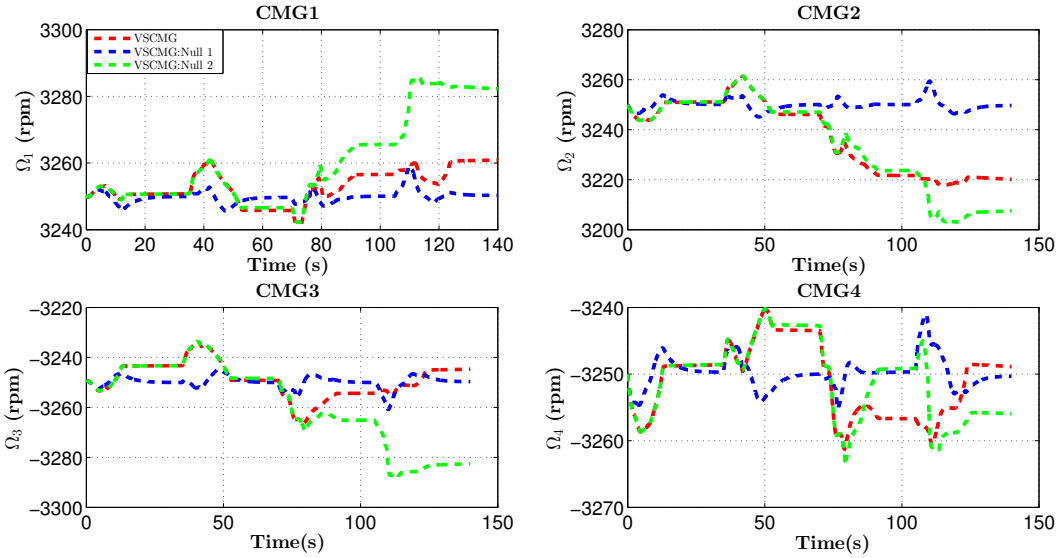

Fig. 21 Wheel speed variation with and without null motion for 4-VSCMG cluster.

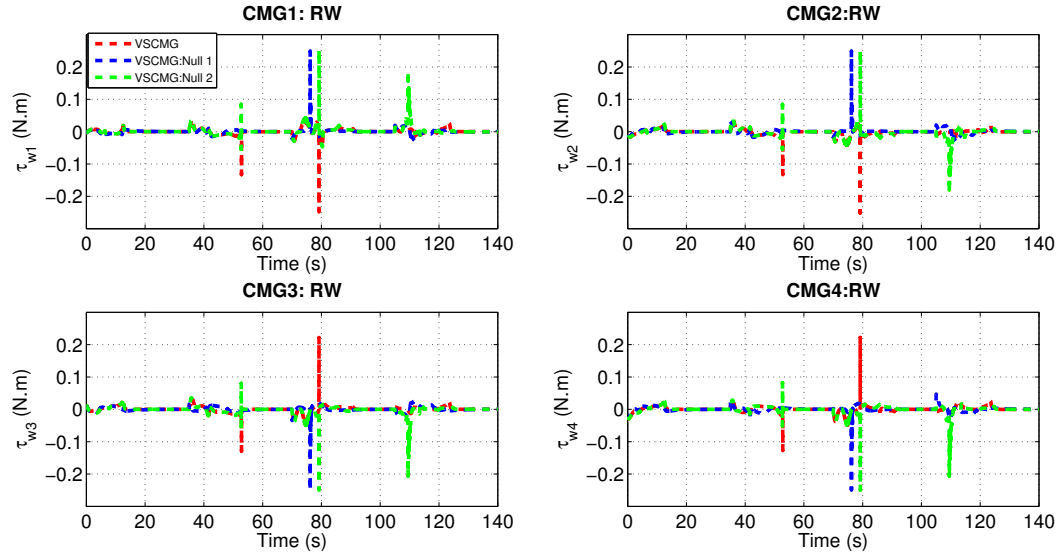

Fig. 22 Wheel torque variation with and without null motion for 4-VSCMG cluster.

C. CMG Based Manoeuvre: With and Without Null Motion

In Section.V.A, the performance of CMG:SDA and VSCMG laws were compared for their effectiveness to complete the multi-target manoeuvre. Subsequently, in Section.V.B, the performance of VSCMG steering laws with and without null motion were studied and analyzed. In this section, null motion (as given in 27) with variable weight (Refer Table.1, $d = 0.75e^{-10m^2}$) is added to the CMG:SDA law and the improvement obtained is explored.

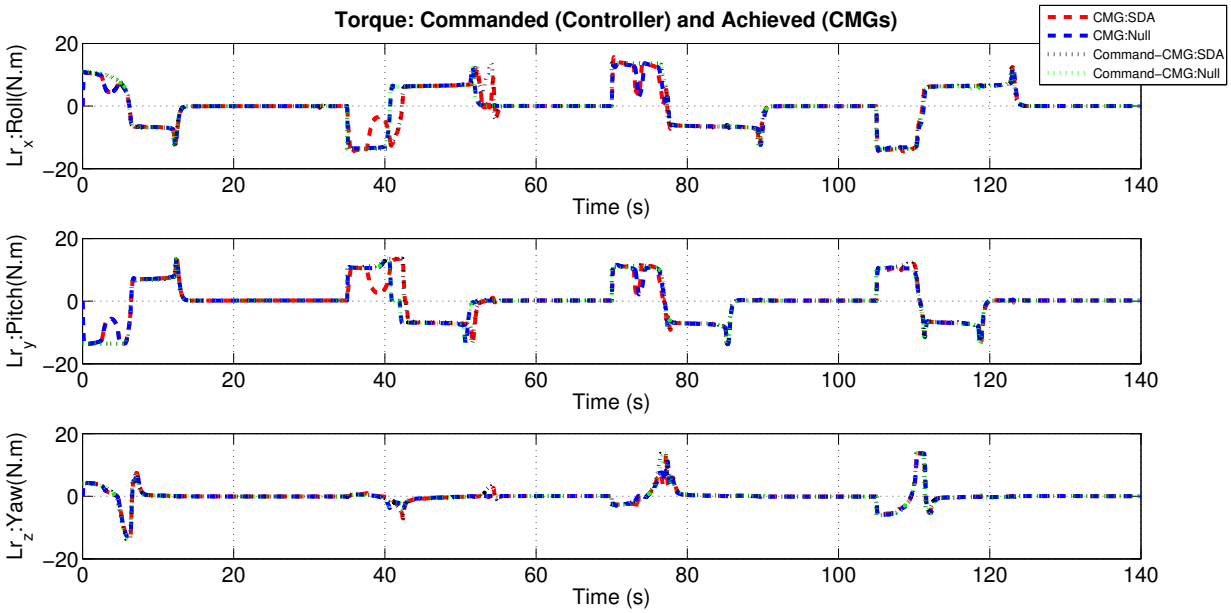

Fig. 23 Commanded and Achieved torques using 4-CMG with SDA law with and without null motion for all four targets

Consider the commanded torque from the controller and the obtained torque from the CMGs shown in Fig.23. Both steering laws, CMG:SDA and CMG:Null entail torque errors. The normalized torque errors for the manoeuvre are shown in Fig.24. Studying the two plots, one observes that for the first target, the torque errors are the same for both steering laws except that there is a blip in the CMG:SDA torque error during tracking at $t = 31$ s, but none for the CMG: Null law. Recall that this led the tracking rate to exceed the threshold for 1.2 seconds. For target 2, the error in CMG:SDA law is greater than that for the CMG:Null. Two peak torque errors occur for CMG:SDA- $\tau_{norm,e} = 0.6$ at $t = 39.7$ s and $t = 54$ s, while the corresponding value for the CMG:Null is $\tau_{norm,e} = 0.3$ at $t = 40.7$ s. For target 3 also, CMG:Null gives a better performance than the CMG:SDA since the former entails a lower torque error. For target 4, the torque error profiles of the two steering laws are nearly the same.

The enlarged view of the demanded and achieved torques about the x-axis by for the CMG:SDA and CMG:Null for target 2 is shown in Fig.25. At $t = 39.2$ s when the demanded torque is -13.6 N.m, CMG:SDA is able to produce just -3.5 N.m only, whereas the CMG:null produced as much as required. Subsequently, as the polarity the torque changed and the magnitude reduced to 6.3 N.m, both steering laws produced the desired torque. Note the jittery response of the

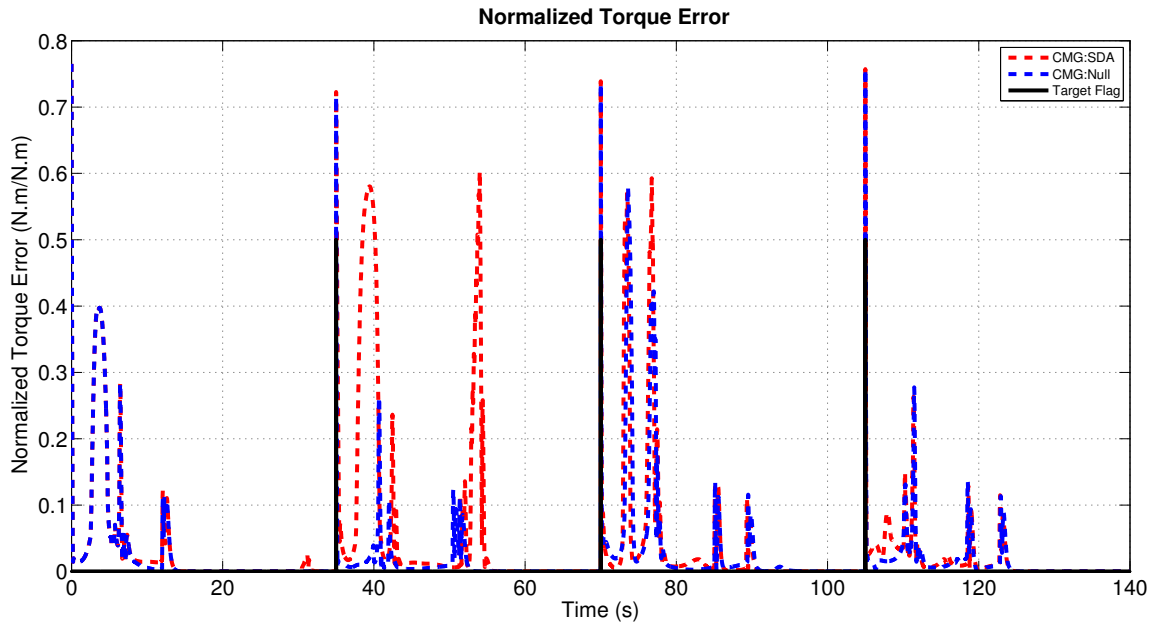

Fig. 24 Normalized torque error using 4-CMG with SDA law with and without null motion for all four targets.

CMG:SDA near the end of the acquisition (at $t \approx 52$s). Owing to the smaller torque error, the CMG:Null steering law enters the tracking phase sooner by 2.6 s (refer to Table.4).

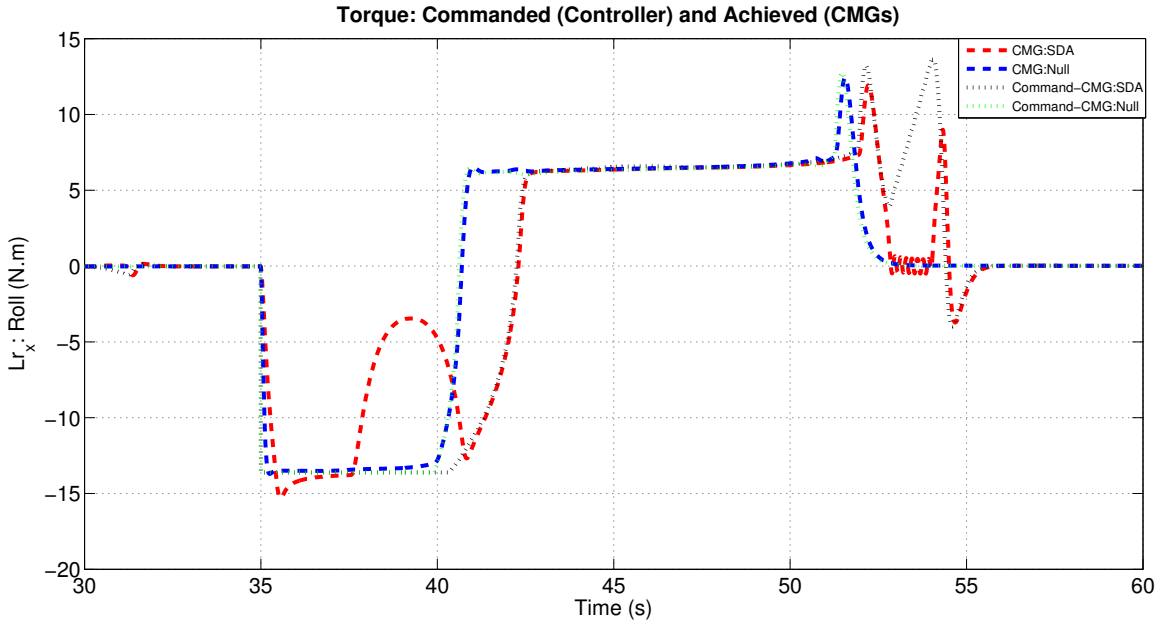

Fig. 25 Commanded and Achieved torques using 4-CMG cluster with SDA law with and without null motion. Torque about the x-axis is enlarged while acquiring and tracking target 2

The singularity indexes m of the CMG:SDA and CMG:null are shown in Fig.26. It is evident at once that the

CMG:SDA is a lot jittery whereas the CMG:Null m is a lot smoother and generally away from $m = 0$. For target 1, they start varying together but starts diverging after $t = 13$ s. The CMG:SDA index falls to $m = 0.001$ at $t = 30.9$ s, which is the reason for the torque error in the tracking phase. For target 2, the CMG:Null law index is high during the high-torque acquisition phase. During $t = 53$ s to $t = 54$ s, the m index for CMG:SDA law decreases to $m = 0.007$ and jitters between $m = 0.007$ to $m = 0.04$. This causes large torque error at the end of the deceleration phase (before entering the tracking phase). For target 3, the singularity indexes of both steering laws oscillates to low values in the beginning ($t = 72$ s to $t = 78$ s). However, the CMG:Null m is relatively farther ($m = 0.01 - 0.1$) from $m = 0$ than the CMG:SDA ($m = 0 - 0.001$). During the tracking phase, the CMG:SDA law has a higher singularity index ($m = 1.2$) than CMG:Null law ($m = 0.35$). Since torque demand is low during tracking phase, CMG:Null doesn't cause a large torque error for this lower m index. For target 4 also, the CMG:SDA law give a higher m index with the lowest value as $m = 0.47$. The corresponding value for CMG:Null law is $m = 0.45$. However, since these values are relatively high, they cause little torque errors as seen in Fig.23 and Fig.24.

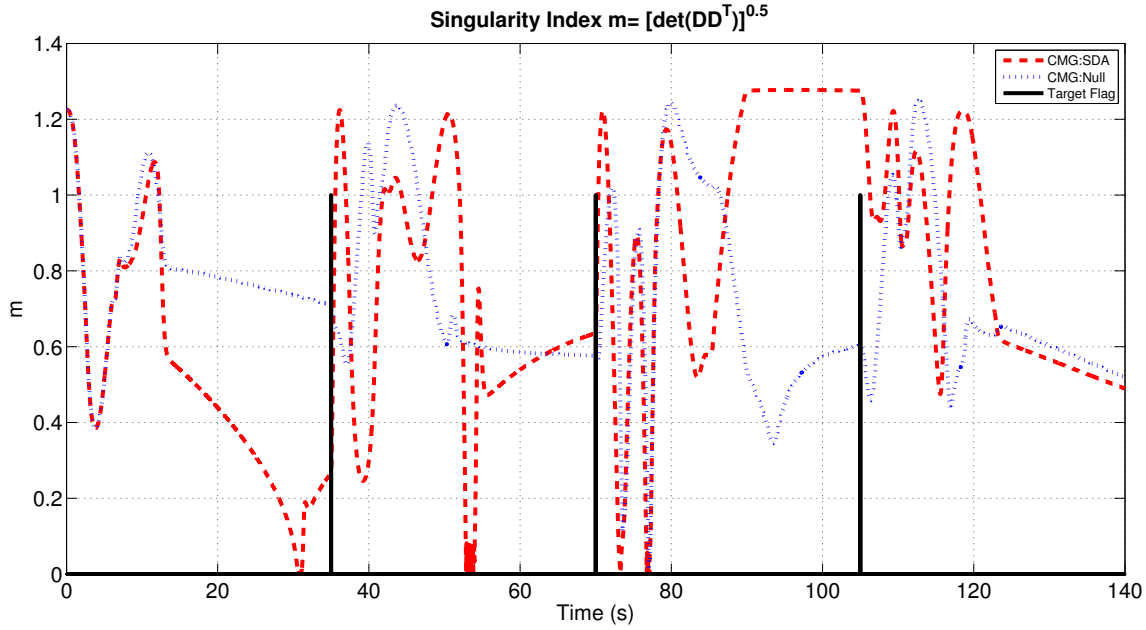

Fig. 26 Singularity Index m variation while using a 4-CMG cluster with SDA law with and without null motion.

The inertial tracking rate and pointing error for CMG:SDA and CMG:Null laws are shown in Fig.27 and Fig.28, where we observe that the CMG:Null perform tracking smoothly whereas the CMG:SDA have occasional blips and jerks which would disturb the payload operation.The comparison of the time required for starting payload operation along with peak normalized torque error is listed in Table.4. The last column giving Δt gives the difference in t_P between CMG:SDA and CMG:Null law. For target 1, the CMG:Null gives 1.2 seconds more payload operation time as the CMG:SDA law transgresses the tracking rate threshold due to singularity. In general, the CMG:Null performs better

than CMG:SDA law (for targets 3 and 4, the gain in time for CMG:SDA is only marginal). For target-2, CMG:Null law attains tracking phase 2.6 seconds sooner than CMG:SDA law.

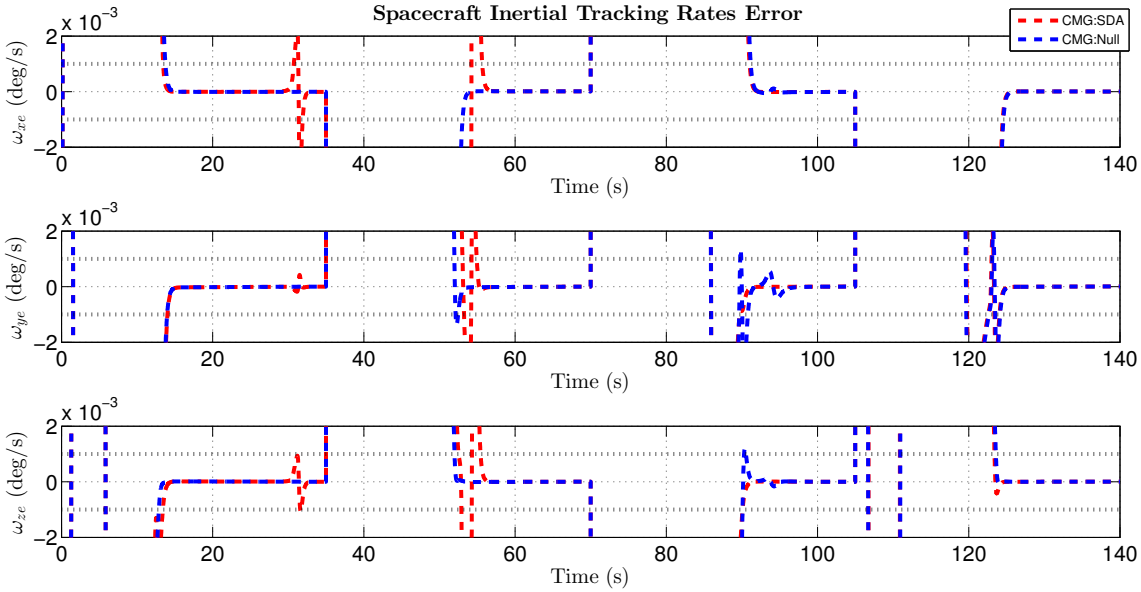

Fig. 27 Inertial tracking rate error while using a 4-CMG cluster with SDA law with and without null motion. Error threshold demanded during tracking is $0.001°/s$ (black dotted line)

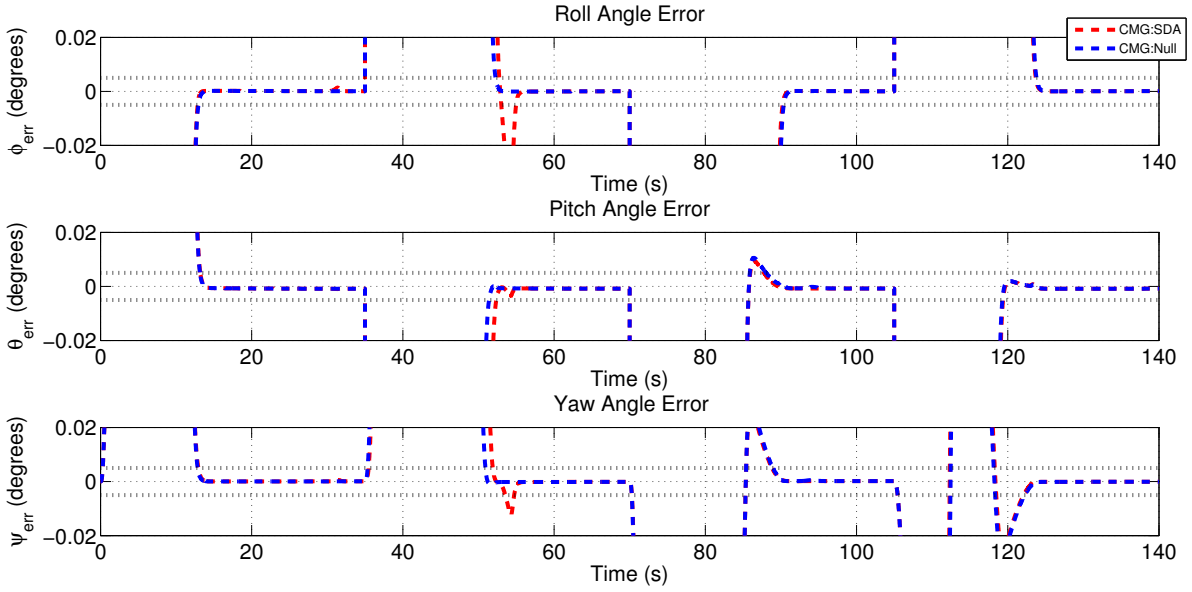

Fig. 28 Euler angle error while using a 4-CMG cluster with SDA law with and without null motion. Error threshold demanded during tracking is $0.005°$ (black dotted line)

Table 4 Comparison of CMG:SDA and CMG:Null steering law while acquiring and tracking four targets

Performance of CMG:SDA and CMG:Null						
Parameters		$\tau_{e,norm}$: max	t_E (s)	t_ω (s)	t_P (s)	Δt (s)
Target-1	**CMG:SDA**	0.4	13.2	14	14*	1.2
	CMG:Null	0.4	13.16	14	14	
Target-2	**CMG:SDA**	0.6	54.98	55.64	55.64	2.6
	CMG:Null	0.26	52.26	53.05	53.05	
Target-3	**CMG:SDA**	0.59	90.23	90.98	90.98	-0.19
	CMG:Null	0.58	90.37	91.17	91.17	
Target-4	**CMG:SDA**	0.26	123.7	124.5	124.5	-0.1
	CMG:Null	0.28	123.8	124.6	124.6	

**CMG:SDA Law exceeds the tracking rate threshold for 1.2 seconds from t = 30.7 s and 31.9s.*

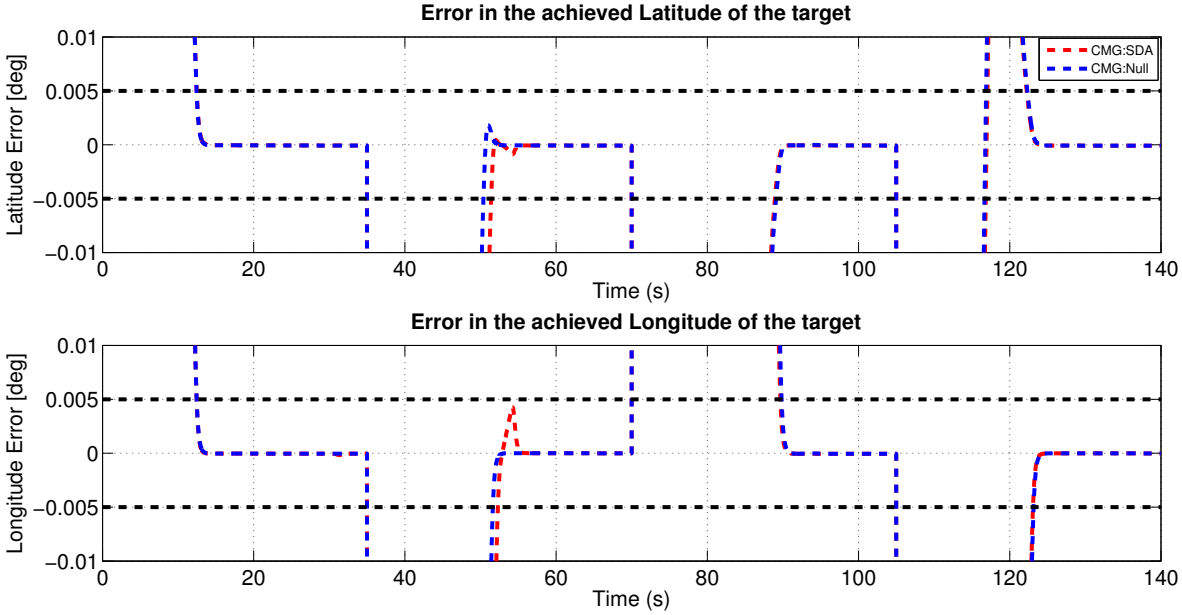

Fig. 29 Error in achieved latitude and longitude values of the targets using a 4-CMG cluster with SDA law with and without null motion.

Fig.29 shows the lat-lon errors in tracking the target for the CMG:SDA and CMG:Null steering laws. As seen earlier, in the pointing error plot (Fig.28), their performance is the same for target-1. For target-2, CMG:Null enters the error threshold sooner than the CMG:SDA law, and the former tracks the targets more smoothly than the latter. For the last two targets their performance is same. The time taken for the tracking rate error to be within the threshold is longer than that required for the pointing error and thus decides the total time available for payload operation.

The gimbal rate profiles are shown in Fig.30. They are feasible, but at t = 53.8s, the gimbal rates computed using

CMG:SDA law are jittery and varies between $\pm 39^\circ/s$ within 0.16s for a total of 1 second for both CMGs 3 and 4. This corresponds to an acceleration of $488^\circ/s^2$. For a typical CMG gimbal inertia of $0.07\, kg.m^2$, the gimbal motor torque required is 0.6 N.m. This is a relatively high magnitude and it will disturb the platform during gimbal operation.

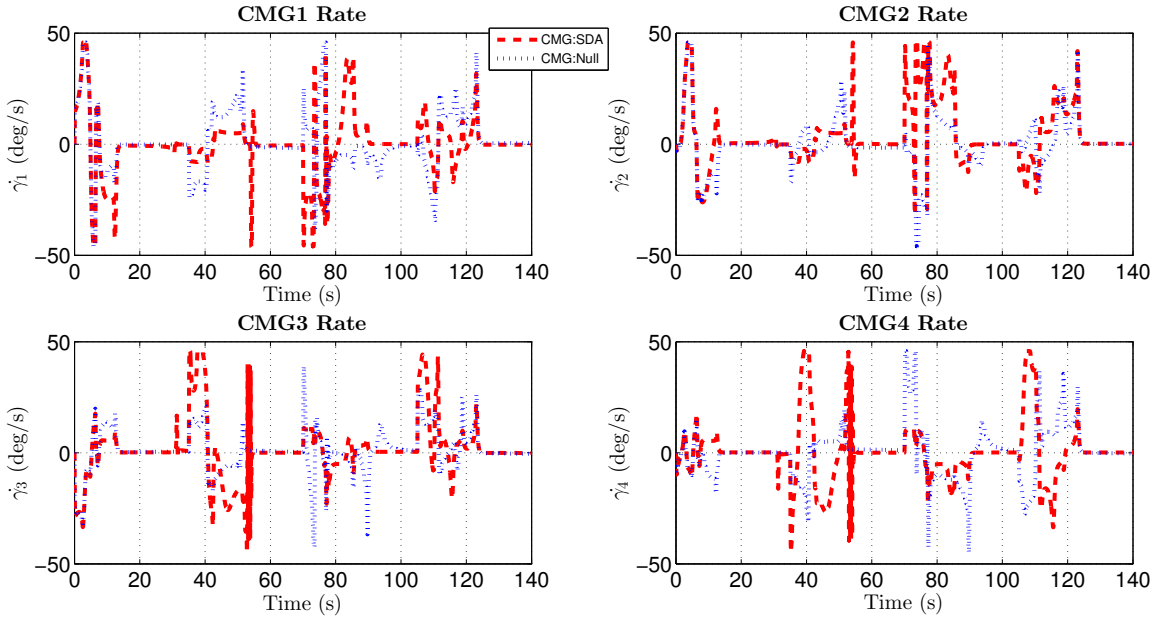

Fig. 30 Gimbal rate history while using a 4-CMG cluster with SDA law with and without null motion.

D. CMGs Vs VSCMGs: With Null Motion

It is seen in the previous sections that VSCMG:Null 1 and CMG:Null gave better performance compared to steering laws without null motion. In this section, the performance and effectiveness of these two laws are compared vis-a-vis normalized torque error and singularity index. Consider the normalized torque error shown in Fig.31. For target 1, the maximum value for VSCMG:Null 1 is $\tau_{norm,e} = 0.82$ against $\tau_{norm,e} = 0.40$ for CMG:Null. The corresponding values for target 2 are 0.63 and 0.26 respectively. Here the time-width of the error for VSCMG: Null 1 is 3 seconds compared to 0.4 second for CMG:Null. Similarly for target 3, maximum torque error for VSCMG:Null 1, $\tau_{norm,e} = 0.84$, is higher than $\tau_{norm,e} = 0.58$ for CMG:Null . The maximum values are comparable for target 4.

The profiles of the singular index m for the two cases are shown in Fig.32. For target 1, the singularity indexes of both VSCMG:Null 1 and CMG:Null laws decrease from their initial values, with the latter to $m = 0.41$ and the former to 0.27. This resulted in a higher torque error for VSCMG: Null 1 in Fig.31. During the end of the acquisition phase and start of the tracking phase, the m index is higher than CMG: Null law. During tracking the values are $m = 1.3$ for VSCMG:Null 1 and $m = 0.58$ for CMG:Null law. The latter is not a low value and, the torque demand during the tracking phase is low and varies between 0.04 N.m to 0.2 N.m only. Hence the performance of both laws are

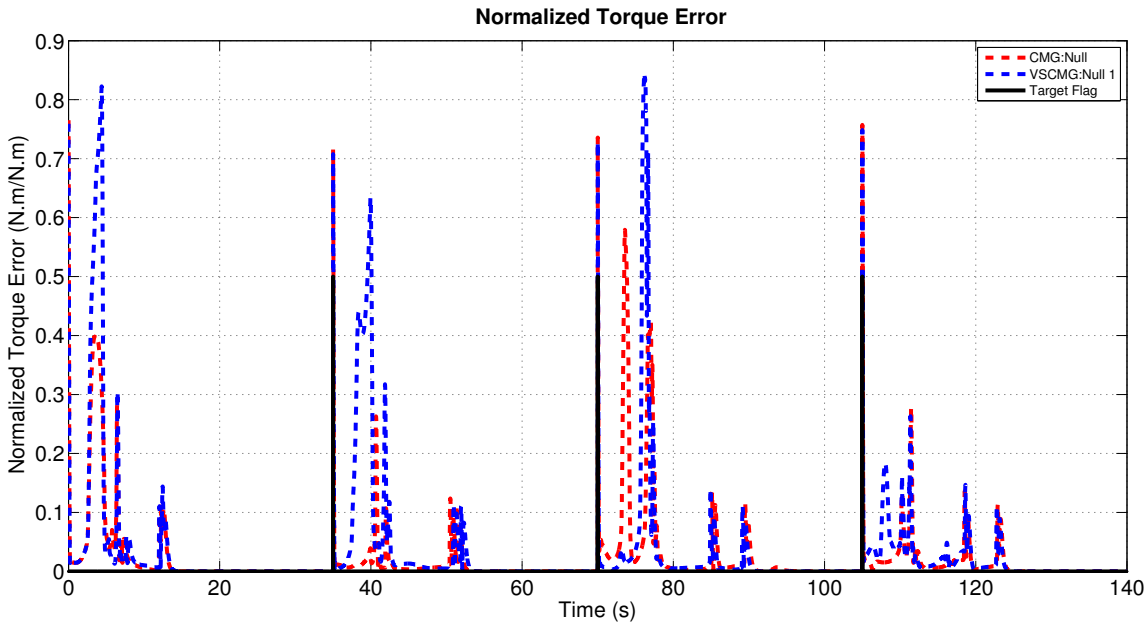

Fig. 31 Normalized torque error comparison of CMG:Null and VSCMG:Null 1 steering law while acquiring and tracking four targets.

comparable in the tracking phase. For the second and third targets, they perform equally in the acquisition phase. Since VSCMG:Null 1 $m < 0.4$ for target 2, it causes a large torque error (-3.5 N.m against the demand of -13.6 N.m, plot is not shown). For target-3 too, the fall in singularity index causes a torque error for both laws: two smaller torque error peaks ($\tau_{norm,e} = 0.57, 0.42$) for CMG:Null law compared to a single large peak for VSCMG:Null 1 ($\tau_{norm,e} = 0.84$). Here the VSCMG:Null 1 has a higher m index than the CMG:Null in the tracking phase, though. The variation in case of target-4 is comparable, which can also be seen from the normalized torque error plot. So, we observe that even though the singularity index m of the VSCMG: Null 1 is, on the average, higher (less singular) than the m of the CMG: Null, the torque error of the VSCMG:Null 1 is still greater than that of the CMG:Null.

VI. Major Observations across all laws

The performance of the following five steering laws is compared in the preceding sections:CMGs with Singularity Direction Avoidance (CMG:SDA), CMGs with SDA-plus-null motion having a variable weight seeking preferred gimbal angles (CMG:Null), VSCMGs using weighted Moore-Penrose pseudoinverse without Null Motion (VSCMG), VSCMG with null motion seeking nominal spin speed and preferred gimbal angles; denoted VSCMG:Null 1, VSCMGs with null motion using gradient of the condition number and nominal spin speed; denoted VSCMG:Null 2. The consolidated salient parameters are listed in Table.5.With no null motion, the CMG:SDA and VSCMG laws are comparable. The tracking performance of VSCMG is better for target 1 and 2, while for the last two targets, the CMG:SDA gives better performance. The gimbal rate jitter occurs in the case of the CMG:SDA law (at $t = 53.8$s) and VSCMG law (at

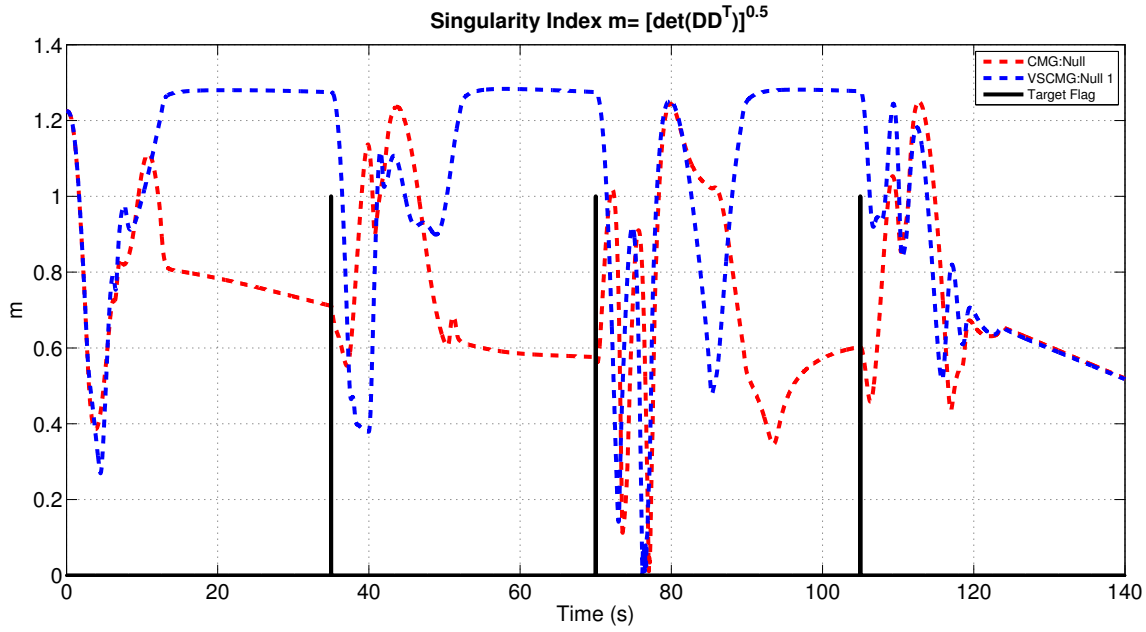

Fig. 32 Singularity Index m comparison of CMG:Null and VSCMG:Null 1 steering law while acquiring and tracking four targets.

t = 75.31 s).

When comparing across VSCMG laws and its variations with addition of null motion, the performance is comparable for the first two targets. The major change is seen for targets 3 and 4, where the tracking commences faster by 1.5 s and 1.8 s for the VSCMG:Null 1 law compared to VSCMG law. For target 4, VSCMG law enters the specified pointing error threshold channel 1.2 s sooner than the VSCMG with null motion based on condition number gradient (VSCMG: Null 2). Gimbal rate oscillations occur once for both VSCMG and VSCMG:Null 2.

The addition of null motion to the CMG:SDA logic results in an overall improvement in performance. The problem of residual tracking error rate going out of threshold for target 1 for the CMG:SDA law is absent here, resulting in a gain of 1.2 s in payload operation. For target 2, CMG:Null law, seeking preferred gimbal angles enters the tracking phase 2.6 s sooner than the CMG:SDA. For the remaining two targets, the performance of the two laws is comparable. The occurrence of gimbal rate oscillations (seen at t = 53.8 s for CMG:SDA) is absent while using CMG:Null seeking the preferred gimbal angles, resulting in the elimination of disturbances to the satellite.

Hence VSCMG:Null 1 and CMG:Null logics were found to be relatively more effective in terms of lower torque error, faster commencement of the tracking phase resulting in a longer payload operation time and absence of jitter in the gimbal rates due to maintaining high singularity index throughout the manoeuvre. The change in the wheel speed for VSCMG:Null 1 law for completing the four target manoeuvre is within ±25 rpm, which is very small (< 1%) compared to the nominal wheel speed of 3250 rpm.

Table 5 Comparison across steering laws while acquiring and tracking four targets sequentially

Steering Law	Parameters	Target-1	Target-2	Target-3	Target-4	Remarks 1
CMG:SDA	m: min	0.0004	0.007	0.00002	0.47	Gimbal rate oscillations
	$\tau_{e,norm} : max$	0.4	0.6	0.59	0.26	
	t_P (s)	14*	55.6	91	124.5	
CMG:Null	m: min	0.41	0.58	0.01	0.43	Gimbal rates smooth
	$\tau_{e,norm} : max$	0.4	0.26	0.58	0.28	
	t_P (s)	14	53.1	91.2	124.6	
VSCMG	m: min	0.27	0.06	0.001	0.03	Gimbal rate oscillations
	$\tau_{e,norm} : max$	0.82	0.58	0.76	0.50	
	t_P (s)	13.9	53.7	92.3	125.1	
VSCMG:Null 1	m: min	0.27	0.38	0.001	0.52	Gimbal rates smooth
	$\tau_{e,norm} : max$	0.82	0.63	0.84	0.26	
	t_P (s)	14.1	53.7	90.8	124.5	
VSCMG:Null 2	m: min	0.27	0.07	0.002	0.14	Gimbal rate oscillations
	$\tau_{e,norm} : max$	0.82	0.58	0.76	0.80	
	t_P (s)	13.9	53.7	92.3	126.3	

**CMG:SDA Law exceeds the tracking rate threshold for 1.2 seconds from* $t = 30.7$ *s and* 31.9*s.*

A. Total momentum error and energy consumed

Clear distinction across steering laws can be obtained by comparing the integral of the torque error (i.e the accumulated momentum error) and integral of the instantaneous total power consumed (i.e the total energy demanded) by the 4-CMG/4-VSCMG cluster. The CMG/VSCMG power will be sum of wheel and its drive electronics power and the gimbal motor power. The wheels will be running at a steady speed for CMGs and will be accelerating and decelerating in case of VSCMGs.

The integral of the torque error is shown in Fig.33 for all the steering laws. Here starting from the target 1, there is a distinction between the CMG and VSCMG steering laws. The VSCMG, VSCMG:Null 1 and VSCMG:Null 2 shows a larger momentum error of 1.6 compared to 1.2 for CMG:SDA and CMG:Null laws. For target 2, momentum error caused due to all the laws increase in the range of 3.1 to 3.7 except for CMG:Null, which increased only to 1.5. The maximum error here is given by the CMG:SDA steering law. For target 3, the momentum error due to VSCMG law is the largest (6.4) and that by CMG:Null is the smallest (2.8). The second, third and fourth positions are taken by VSCMG:Null 1(6.3), CMG:SDA(5.06) and VSCMG:Null 1 (4.35) respectively. As we proceed with the acquisition and tracking of target-4, the VSCMG:Null 2 law gives the biggest error and CMG:Null the lowest. The peak momentum errors of the steering laws are listed in Table.6.

Similarly the total energy consumed for the 4-CMG cluster in illustrated in Fig.34. Wheels are accelerated and

decelerated during VSCMG operations along with the gimbal rotation. Hence the energy consumed by all VSCMG control laws are more. The mean of the peak energies consumed by CMG:SDA and CMG: Null is 5380 W-s compared to 6250 W-s for VSCMG, VSCMG:Null 1 and VSCMG:Null 2 (an increase of 16.2%). The lowest momentum error among the VSCMGs steering laws is obtained from VSCMG:Null 1 (refer to Table.6 ,5.1) and between the CMG steering laws is for CMG:Null (3.3). However, the VSCMG:Null 1 consumes 8.7% more energy than CMG:Null law.

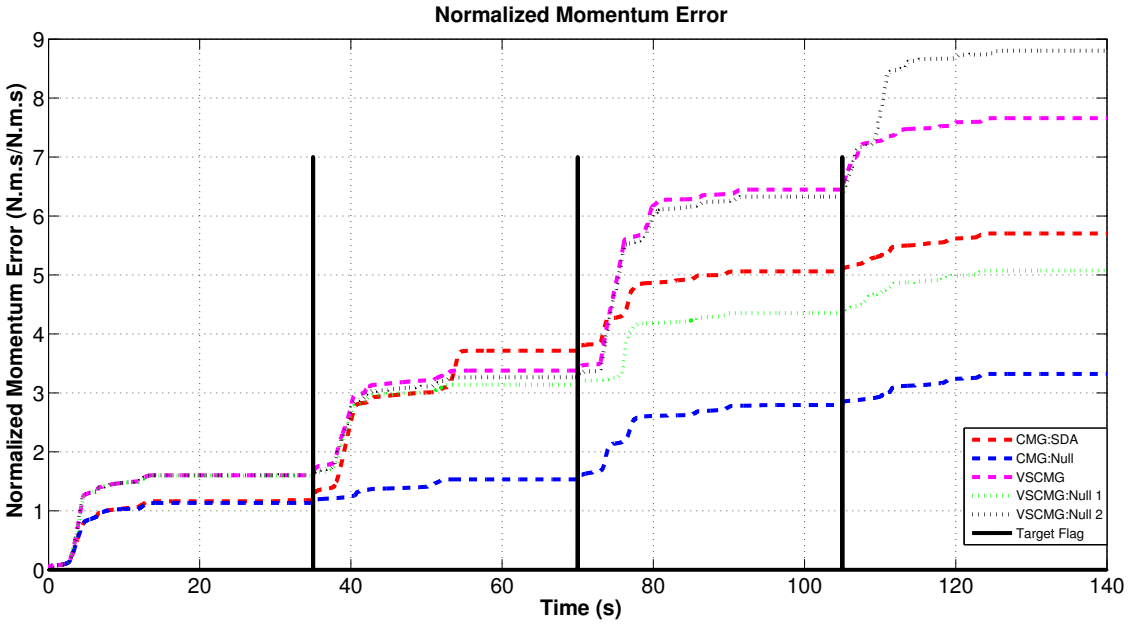

Fig. 33 Integral of the normalized torque error for five steering laws- CMG, CMG: Null, VSCMG, VSCMG: Null 1, VSCMG: Null 2 while acquiring and tracking 4 targets.

VII. Conclusions

The problem of multiple landmark acquisition and tracking is studied using a constant or variable speed 4-CMG assembly in a roof type configuration using five type of steering laws: CMGs with Singularity Direction Avoidance (CMG:SDA), CMGs with SDA-plus-null motion having a variable weight seeking preferred gimbal angles (CMG:Null), VSCMGs using weighted Moore-Penrose pseudoinverse without Null Motion (VSCMG), VSCMG with null motion seeking nominal spin speed and preferred gimbal angles; denoted VSCMG:Null 1, VSCMGs with null motion using gradient of the condition number and nominal spin speed; denoted VSCMG:Null 2. Under the same set of target distribution and outer-loop attitude controller their performance was compared based on normalized torque error, singularity index and pointing error. The CMGs with singularity direction avoidance and VSCMGs using weighted Moore-Penrose pseudoinverse perform comparably. The addition of null motion, especially the one in which preferred gimbal angles and wheel speeds were used (VSCMG:Null 1) is seen to be effective in reducing the torque error, keeping the configuration away from singularity, and longer target tracking, with no jitter in the gimbal rates. It also demands

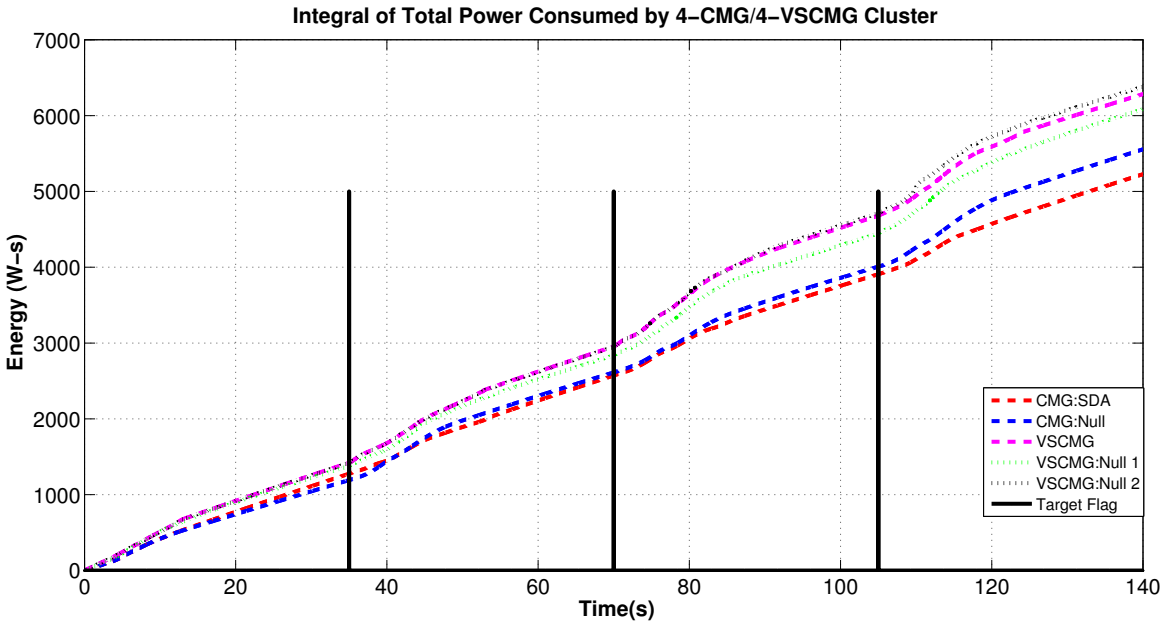

Fig. 34 Integral of the total power consumed for five steering laws- CMG, CMG: Null, VSCMG, VSCMG: Null 1, VSCMG: Null 2 while acquiring and tracking 4 targets.

Table 6 Total energy consumed and momentum error comparison across steering laws while acquiring and tracking four targets sequentially at the end of manoeuvre

Steering Law	Total Energy Consumed (W-s)	Integral of torque error (N.m.s)	Remarks
CMG:SDA	5527	5.7	**Energy: Lowest , Error: Medium**
CMG:Null	5556	3.3	**Energy: Low , Error: Lowest**
VSCMG	6284	7.7	**Energy: High, Error: High**
VSCMG:Null 1	6085	5.1	**Energy: Medium, Error: Medium**
VSCMG:Null 2	6382	8.8	**Energy: Highest, Error: Highest**

lesser wheel speed variation for singularity avoidance than other VSCMG laws. The performance of CMG:SDA (Singular Direction Avoidance) law is improved by the addition of null motion based on preferred gimbal angles (CMG:Null law). Lastly the integral of the normalized torque error and total energy consumed was compared across the steering laws. This showed a clear distinction between the VSCMG and CMG laws. The CMG:Null law gave the lowest momentum error (62.5% less than VSCMG:Null 2) and consumed relatively less energy (13% less than VSCMG:Null 2). Among the VSCMG steering laws, VSCMG:Null 1 performs better with 42.5% less momentum error and 4.7% less energy compared to VSCMG:Null 2. However CMG:Null consumes 8.7% less energy and 35.2% less momentum error relative to VSCMG:Null 1. Hence in terms of better singularity index, low torque and momentum error, faster commencement of paylaod operation, smother gimbal rate and relatively less energy consumption, CMG:Null has a distinct advantage over other control laws.

From this study it is concluded that, for an effective assessment of the CMG/VSCMGs steering laws, performance should be compared across various parameters. The singularity index and torque error alone are not enough and other parameters such as the pointing and rate errors decreasing to their respective threshold channels, avoiding jitter in gimbal rates, momentum error and total energy consumption are equally significant. The addition of null motion improves the performance of the steering law of the CMGs using singularity direction avoidance, and of the VSCMGs using Moore-Penrose pseudoinverse. It is found that it is advantageous and recommended to apply the steering laws along with appropriate null gimbal rates. If one wishes to implement a simpler on-board control algorithm, CMG:Null steering logic is preferred to VSCMG:Null 1 steering logic. In addition, CMG:Null steering law shows a distinct advantage over all other laws based on multiple performance parameters and is an ideal choice for on-board implementation.

References

[1] Honeywell, "HR04 Reaction Wheel System: Data Sheet," , 2018. doi:https://aerospace.honeywell.com/content/dam/aerobt/en/documents/learn/products/sensors/brochures/N61-1586-000-001_HR04_RWA_17012018-bro.pdf.

[2] Honeywell, "Constellation Series Reaction Wheels: Data Sheet," , 2003. doi:ftp://apollo.ssl.berkeley.edu/pub/Pointing_Studies/Hardware/Honeywell%20Reaction%20Wheels.pdf.

[3] Airbus, "Airbus CMG 15-45S: Data Sheet," , 2014. doi:https://satsearch.co/products/airbus-defence-and-space-cmg-15-45s.

[4] Honeywell, "M50 Control Moment Gyro: Data Sheet," , 2002. doi:https://satcatalog.s3.amazonaws.com/components/6/SatCatalog_-_Honeywell_-_M50_CMG_-_Datasheet.pdf?lastmod=20210708012029.

[5] Bedrossian, N. S., Paradiso, J., Bergmann, E. V., and Rowell, D., "Steering law design for redundant single-gimbal control moment gyroscopes," *Journal of Guidance, Control, and Dynamics*, Vol. 13, No. 6, 1990, pp. 1083–1089. doi:10.2514/3.20582.

[6] Lappas, V. J., "A control moment gyro (CMG) based attitude control system (ACS) for agile small satellites," Ph.D. thesis,

University of Surrey, 2002. doi:https://www.proquest.com/openview/41afd0570cf67b5696d087f7b999d46a/1?pq-origsite=gscholar&cbl=51922&diss=y.

[7] Leve, F. A., Hamilton, B. J., and Peck, M. A., *Spacecraft Momentum Control Systems*, Springer International Publishing, 2015. doi:10.1007/978-3-319-22563-0.

[8] Margulies, G., and Aubrun, J., "Geometric theory of single-gimbal control moment gyro systems," *AIAA Guidance and Control Conference, San Diego, California*, 1976, pp. 255–267. Paper 76-1945.

[9] Wie, B., Bailey, D., and Heiberg, C., "Singularity Robust Steering Logic for Redundant Single-Gimbal Control Moment Gyros," *Journal of Guidance, Control, and Dynamics*, Vol. 24, No. 5, 2001, pp. 865–872. doi:10.2514/2.4799.

[10] YAVUZOĞLU, E., "Steering laws for control moment gyroscope systems used in spacecrafts attitude control," , 2003. doi:http://citeseerx.ist.psu.edu/viewdoc/download?doi=10.1.1.456.9082&rep=rep1&type=pdf.

[11] Nakamura, Y., and Hanafusa, H., "Inverse Kinematic Solutions With Singularity Robustness for Robot Manipulator Control," *Journal of Dynamic Systems, Measurement, and Control*, Vol. 108, No. 3, 1986, p. 163. doi:10.1115/1.3143764.

[12] Ford, K. A., and Hall, C. D., "Singular direction avoidance steering for control-moment gyros," *Journal of Guidance, Control, and Dynamics*, Vol. 23, No. 4, 2000, pp. 648–656. doi:https://doi.org/10.2514/2.4610.

[13] Leve, F. A., and Fitz-Coy, N. G., "Hybrid steering logic for single-gimbal control moment gyroscopes," *Journal of guidance, control, and dynamics*, Vol. 33, No. 4, 2010, pp. 1202–1212. doi:https://doi.org/10.2514/1.46853.

[14] VADALI, S. R., WALKER, S. R., and OH, H.-S., "Preferred gimbal angles for single gimbal control moment gyros," *Journal of Guidance, Control, and Dynamics*, Vol. 13, No. 6, 1990, pp. 1090–1095. doi:10.2514/3.20583.

[15] Lappas, V., and Wie, B., "Robust control moment gyroscope steering logic with gimbal angle constraints," *Journal of guidance, control, and dynamics*, Vol. 32, No. 5, 2009, pp. 1662–1666. doi:https://doi.org/10.2514/1.43806.

[16] Mony, A., "RRT-Based Steering Law for Singularity Avoidance of Control Moment Gyros used for Spacecraft Target Acquisition," *Proceedings of the Indian Control Conference, IIT Hyderabad*, 2019, pp. 361–366. doi:https://doi.org/10.1109/ICC47138.2019.9123199.

[17] Schaub, H., Vadali, S. R., Junkins, J. L., et al., "Feedback control law for variable speed control moment gyros," *Journal of the Astronautical Sciences*, Vol. 46, No. 3, 1998, pp. 307–328. doi:https://doi.org/10.1007/BF03546239.

[18] Schaub, H., and Junkins, J. L., *Analytical mechanics of space systems- Chapter 8, Sec 8.8*, American Institute of Aeronautics and Astronautics, 2015. doi:https://doi.org/10.2514/4.105210.

[19] Wie, B., *Space Vehicle Dynamics and Control, Second Edition, Chapter 11*, American Institute of Aeronautics and Astronautics, 2008. doi:10.2514/4.860119.

[20] Hablani, H. B., "Design of Payload Control System for Tracking Moving Objects," *Journal of Guidance, Control and Dynamics*, Vol. 12, No. 3, 1989, pp. 365–374. doi:https://doi.org/10.2514/3.20417.

[21] Wie, B., Bailey, D., and Heiberg, C., "Rapid multitarget acquisition and pointing control of agile spacecraft," *Journal of Guidance, Control, and Dynamics*, Vol. 25, No. 1, 2002, pp. 96–104. doi:https://doi.org/10.2514/2.4854.

[22] Oliver, M., and Eberhard, G., *Satellite orbits:. Models, Methods and applications*, Springer, 2000. doi:https://doi.org/10.1115/1.1451162.

[23] Markley, F. L., "Fast Quaternion Estimation from Two Vector Measurements," *Journal of Guidance, Control, and Dynamics*, Vol. 25, No. 2, 2002, pp. 411–414. doi:https://doi.org/10.2514/2.4897.

[24] Hughes, P. C., *Spacecraft attitude dynamics*, Courier Dover Publications, 2012.

[25] Wie, B., Weiss, H., and Arapostathis, A., "Quarternion feedback regulator for spacecraft eigenaxis rotations," *Journal of Guidance, Control, and Dynamics*, Vol. 12, No. 3, 1989, pp. 375–380. doi:https://doi.org/10.2514/3.20418.

[26] Wertz, J. R., *Spacecraft attitude determination and control*, Vol. 73, Springer Science & Business Media, 2012. doi:https://doi.org/10.1007/978-94-009-9907-7.

[27] Larson, W. J., and Wertz, J. R., "Space mission analysis and design," Tech. rep., Torrance, CA (United States); Microcosm, Inc., 1992.

[28] Pritchard, W. L., and Sciulli, J. A., *Satellite communication systems engineering*, Prentice-Hall, Inc., 1986.

[29] Kumar, S., and Hablani, H. B., "REMOTE SENSING SCANNING MIRROR CONTROLLER DESIGN,M.Tech Thesis, Department of Aerospace Engineering," , 2011.

[30] Hablani, H. B., *AE:626 Spacecraft Attitude Dynamics and Control*, Course Material, 2013.

[31] Mony, A., Hablani, H., and Sharma, G., "Control Moment Gyro (CMG) Sizing and Cluster Configuration Selection for Agile Spacecraft," *10th National Symposium and Exhibition on Aerospace and Related Mechanisms (ARMS 2016)*, 2016. doi:https://www.researchgate.net/publication/311665872_Control_Moment_Gyro_CMG_Sizing_and_Cluster_Configuration_Selection_for_Agile_Spacecraft.